Icarus 328 (2019) 160–175

Contents lists available at ScienceDirect

Icarus

journal homepage: www.elsevier.com/locate/icarus

Update of the HITRAN collision-induced absorption section

Tijs Karman[a,b,c], Iouli E. Gordon[a,*], Ad van der Avoird[b], Yury I. Baranov[d,1], Christian Boulet[e], Brian J. Drouin[f], Gerrit C. Groenenboom[b], Magnus Gustafsson[g], Jean-Michel Hartmann[h], Robert L. Kurucz[a], Laurence S. Rothman[a], Kang Sun[a,k], Keeyoon Sung[f], Ryan Thalman[i,j], Ha Tran[l], Edward H. Wishnow[m], Robin Wordsworth[n], Andrey A. Vigasin[o], Rainer Volkamer[i], Wim J. van der Zande[b]

[a] Harvard-Smithsonian Center for Astrophysics, Atomic and Molecular Physics Division, Cambridge, MA, USA
[b] Institute for Molecules and Materials, Radboud University, Heyendaalseweg 135, 6525, AJ, Nijmegen, the Netherlands
[c] Durham University, South Road, Durham DH1 3LE, United Kingdom
[d] SPA "Typhoon", Institute of Experimental Meteorology, 4 Pobeda Street, Obninsk, Kaluga Reg. 2490338, Russia
[e] Institut des Sciences Moléculaires d'Orsay, CNRS, Université Paris-Sud, Université Paris-Saclay, Orsay F-91405, France
[f] Jet Propulsion Laboratory, Caltech, Pasadena, CA, USA
[g] Applied Physics, Division of Materials Science, Department of Engineering Science and Mathematics, Luleå University of Technology, SE-97187 Luleå, Sweden
[h] Laboratoire de Météorologie Dynamique/IPSL, CNRS, École polytechnique, Sorbonne Université, École normale supérieure, PSL Research University, F-91120 Palaiseau, France
[i] Department of Chemistry & CIRES, University of Colorado Boulder, Boulder, CO, USA
[j] Department of Chemistry, Snow College, Ephraim, UT, USA
[k] Research and Education in eNergy, Environment and Water Institute, University at Buffalo, Buffalo, NY, USA
[l] Laboratoire de Météorologie Dynamique/IPSL, CNRS, Sorbonne Université, École normale supérieure, PSL Research University, École polytechnique, F-75005 Paris, France
[m] University of California Berkeley, Space Sciences Laboratory, 7 Gauss Way, Berkeley, CA, USA
[n] Department of Earth and Planetary Sciences, Harvard University, Cambridge, MA, USA
[o] Obukhov Institute of Atmospheric Physics, Russian Academy of Sciences, Pyzhevsky per. 3, 119017 Moscow, Russia

A B S T R A C T

Correct parameterization of the Collision-induced Absorption (CIA) phenomena is essential for accurate modeling of planetary atmospheres. The HITRAN spectroscopic database provides these parameters in a dedicated section. Here, we significantly revise and extend the HITRAN CIA data with respect to the original effort described in Richard et al. [JQSRT **113**, 1276 (2012)]. The extension concerns new collisional pairs as well as wider spectral and temperature ranges for the existing pairs. The database now contains CIA for N_2-N_2, N_2-H_2, N_2-CH_4, N_2-H_2O, N_2-O_2, O_2-O_2, O_2-CO_2, CO_2-CO_2, H_2-H_2, H_2-He, H_2-CH_4, H_2-H, H-He, CH_4-CH_4, CH_4-CO_2, CH_4-He, and CH_4-Ar collision pairs. The sources of data as well as their validation and selection are discussed. A wish list to eliminate remaining deficiencies or lack of data from the astrophysics perspective is also presented.

1. Introduction

Collision-Induced Absorption (CIA) of infrared radiation contributes appreciably to the total absorption of radiation in planetary atmospheres. Indeed, even gases that consist of molecules that have no intrinsic electric dipole moment (including molecular hydrogen, oxygen and nitrogen) absorb radiation if densities are sufficiently high. In the terrestrial atmosphere N_2-N_2, N_2-O_2, and O_2-O_2 collision complexes are important absorbers at various wavelengths and are routinely monitored by different remote sensing (Sioris et al., 2014 Chimot et al., 2017 Kataoka et al., 2017) and ground-based missions (Hartmann et al., 2017 Ortega et al., 2016 Spinei et al., 2014 Gordon et al., 2010). Interestingly, O_2-O_2 absorption in the visible and near infrared is targeted as a biomarker on potentially habitable exoplanets (Meadows, 2017). Naturally, since hydrogen and helium gases dominate the atmospheres of gas giants and brown dwarfs, absorption in these atmospheres has a large contribution due to collision complexes such as H_2-H_2, H_2-He, as well as other X-H_2 and X-He complexes, where X represents other abundant molecules such as CH_4. Furthermore, knowledge of X-N_2 CIA is required for modeling of the atmospheres of Titan and other nitrogen-rich worlds, and X-CO_2 for Venus and exoplanets with pronounced volcanic activity. Because of the diversity of exoplanetary atmospheres

* Corresponding author.
E-mail addresses: tijs.karman@cfa.harvard.edu (T. Karman), igordon@cfa.harvard.edu (I.E. Gordon).
[1] Deceased on July 7, 2018

https://doi.org/10.1016/j.icarus.2019.02.034
Received 30 October 2018; Received in revised form 15 February 2019; Accepted 26 February 2019
Available online 14 March 2019
0019-1035/

in their constituents and thermodynamic conditions, one needs to know collision-induced absorption parameters over wide ranges of temperatures for many collisional pairs. We refer the reader to Hartmann et al. (2018a) for a recent review of pressure-induced effects on molecular spectroscopy.

The HITRAN spectroscopic database is the primary source of data for interpretation of spectral atmospheric retrievals of planetary atmospheres and is an important input to radiative transfer codes. The most recent edition of the database, HITRAN 2016 (Gordon et al., 2017), presents several types of data. It consists of line-by-line lists, experimental absorption cross sections, CIA data and aerosol indices of refraction. The CIA section is a relatively recent addition to the database and was introduced only in the 2012 edition for several collisional partners, (Rothman et al., 2013) namely N_2-N_2, N_2-H_2, N_2-CH_4, N_2-O_2, O_2-O_2, O_2-CO_2, CO_2-CO_2, H_2-H_2, H_2-He, H_2-CH_4, H_2-H, H-He, CH_4-CH_4, and CH_4-Ar. The details are given in Richard et al. (2012), where various calculations and measurements of CIA available in the literature at that time were evaluated, selected, and put into a consistent format. The HITRAN CIA data have received a warm welcome from the scientific community and proved invaluable for modeling and interpreting spectra of planetary atmospheres. It has been integrated into numerous radiative transfer codes for (exo)planetary research, see for instance (Hollis et al., 2013; Schreier et al., 2014; Lora et al., 2015; Malik et al., 2017; Gandhi and Madhusudhan, 2018; Dudhia, 2017).

There are multiple requests from the communities of atmospheric and planetary scientists to extend the work of Richard et al. further. The recent white paper by Fortney et al. (2016) addresses the needs for reference atomic and molecular data from the exoplanetary perspective. The authors specifically call for the extension of the HITRAN CIA section. In this work we make use of recent advances in experimental and theoretical works devoted to the studies of the collision-induced absorption relevant to planetary atmospheres and a) update data for already existing collisional systems by improving the accuracy and extending spectral and temperature ranges; b) add data for the collisional systems CO_2-H_2, CO_2-CH_4, CO_2-He, N_2-He, CH_4-He, and N_2-H_2O. The sources of data and their choices are discussed in detail. Fig. 1 contains a graphical representation of the data contained in the HITRAN CIA section, indicating which bands for each collisional pair are available, newly added or updated. More details about the spectral and temperature range for the bands included for each collisional pair can be found in Table 1. At the end of this paper we discuss the remaining challenges in available reference parameters and present a wish-list from an astrophysical perspective.

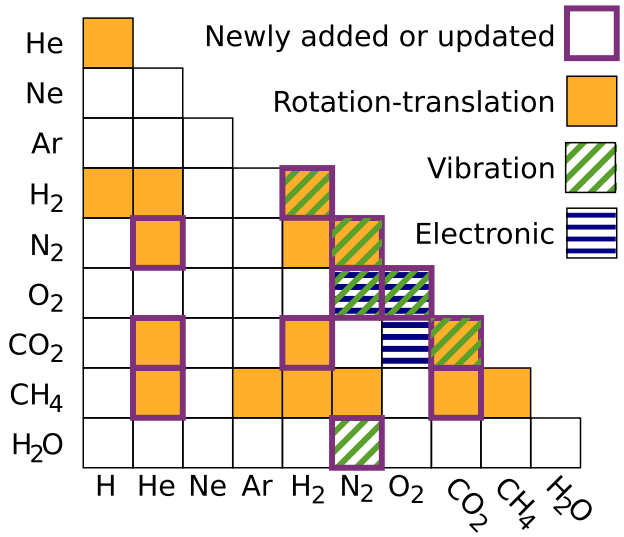

Fig. 1. A graphical representation of the data available for each collisional pair, where the color coding indicates the nature of the bands included. Orange fill indicates that data for the roto-translational band are included, diagonal stripes indicate data for vibrational bands are available, and horizontal stripes indicate data for electronic bands are included. Squares corresponding to newly added and updated systems are marked with thick palatinate boundaries. Blank squares indicate data not yet available, indicating directions for future work.

As in the original effort described in Richard et al. (2012), only binary collisions are considered. We continue to provide "Main" and "Alternate" folders. The Main folder contains recommended sets of collision-induced absorptions whereas the Alternate folder contains two types of data. One type of data is simply alternative to that in the Main folder, in particular where the CIA parameterization is intended to be used in conjunction with a specific line-by-line list. This is the case for O_2-Air absorption in particular, see Section 3.6 for details. A second type of data in the "Alternate" folder is provided when the data are not generally recommended due to large uncertainties, and should be used with caution, but the data have a clear advantage over the recommended set for specific applications, *e.g.* extended temperature ranges or to account for spin statistics.

Instructions for accessing the database can be found on the HITRAN website (www.hitran.org/cia).

2. General definitions

The attenuation of light by a gas with absorption coefficient $k(\nu)$ is given by the Lambert law (excluding the contribution of Rayleigh scattering)

$$-\ln[T(\nu)] = k(\nu)L, \tag{1}$$

where $T(\nu)$ is the transmittance at wavenumber ν and L is the optical path length. Leaving aside pressure variations in the line shape of resonant transitions of an individual molecule, the absorption coefficient is given by the virial expansion in the number density ρ

$$k(\nu) = k^{(1)}(\nu)\,\rho + k^{(2)}(\nu)\,\rho^2 + ..., \tag{2}$$

which permits discrimination of monomer absorption and absorption by molecular pairs or ternary and larger complexes of colliding molecules. The absorption by collision complexes involving more than two molecules is expected to be insignificant under typical atmospheric conditions, even for planets with dense atmospheres such as Venus, and is thus disregarded here.

The HITRAN-tabulated CIA absorption coefficients contain contributions of all binary complexes, bound, quasi-bound, and free scattering states, although the name *collision*-induced absorption suggests it exclusively applies to unbound scattering states only. This has been the source of some debate – in which we do not wish to engage here – but it may be important to note that in principle the tabulated absorption coefficients are not missing contributions of "truly bound" states, *i.e.*, these should not be double-counted by adding them separately.

In HITRAN units, the density ρ is given in molecule cm^{-3}. The monomer absorption cross section $k^{(1)}(\nu)$ is given in cm^2 $molecule^{-1}$, and is tabulated in HITRAN for many atmospherically relevant molecules. The contribution of binary complexes is given by the CIA absorption coefficient, $k^{(2)}(\nu)$, which is tabulated in the HITRAN CIA section discussed in this paper, in units of cm^5 $molecule^{-2}$. The wavenumber and absorption coefficient are tabulated in two-column format, where each band and temperature set is preceded by a header, formatted as defined in Fig. 2. In the collision-induced absorption literature, number densities are usually expressed in amagats, the number density of an ideal gas at standard temperature and pressure. The absorption coefficients can be converted as

$$k(\mathrm{cm^5\ molecule^{-2}}) = 1.385277\ 10^{-39}\alpha(\mathrm{cm^{-1}amagat^{-2}}) \tag{3}$$

where α and k represent the binary absorption coefficients in $cm^{-1}amagat^{-2}$ and cm^5 $molecule^{-2}$, respectively.

For mixtures containing multiple molecular species, for example A

Table 1
Summary of the different bands available in the HITRAN CIA Main and Alternate folders for all collisional systems. The "band description" specifies which (forbidden) monomer transitions the data set corresponds to and, where ambiguous, of which monomer.
*See Fig. 5 for the assignment of the transitions.

System	Folder	ν range (cm^{-1})	T range (K)	# of sets	Band description	Ref.
$H_2 - H_2$	Main	20–10,000	200–3000	113	Roto-translational, fundamental, 1st overtone	(Abel et al., 2011)
	Alternate	0–2400	40–400	120	Roto-translational	(Fletcher et al., 2018)
H_2-He	Main	20–20,000	200–9900	334	Roto-translational fundamental, 1st–4th overtone	(Abel et al., 2012a)
H_2-H	Main	100–10,000	1000–2500	4	Roto-translational, fundamental, 1st overtone	(Gustafsson and Frommhold, 2003)
He-H	Main	50–11,000	1500–10,000	10	Roto-translational, fundamental, 1st overtone	(Gustafsson and Frommhold, 2001)
$H_2 - CH_4$	Main	0–1946	40–400	10	Roto-translational	(Borysow and Frommhold, 1986a)
N_2-He	Main	1–1000	300	1	Roto-translational	(Bar-Ziv and Weiss, 1972)
CO_2-He	Main	0–1000	300	1	Roto-translational	(Bar-Ziv and Weiss, 1972)
CH_4-He	Main	1–1000	40–350	10	Roto-translational	(Taylor et al., 1988)
CH_4-Ar	Alternate	1–697	70–296	5	Roto-translational	(Samuelson et al., 1997)
$CH_4 - CH_4$	Alternate	0–990	200–800	7	Roto-translational	(Borysow and Frommhold, 1987)
$CO_2 - H_2$	Main	0–2000	200–350	4	Roto-translational	(Wordsworth et al., 2017)
$CO_2 - CH_4$	Main	1–2000	200–350	4	Roto-translational	(Wordsworth et al., 2017)
$CO_2 - CO_2$	Main	1–750	200–800	10	Roto-translational	(Gruszka and Borysow, 1997)
		1000–1800	200–350	6	Fermi dyad	(Baranov and Vigasin, 1999)
		2510–2850	221–297	3	Fermi triad	(Baranov et al., 2003a)
		2850–3250	298	1	$\nu_2 + \nu_3$ band	(Baranov, 2018)
$N_2 - H_2$	Main	0–1886	40–400	10	Roto-translational	(Borysow and Frommhold, 1986b)
$N_2 - N_2$	Main	0–554	200–309	9	Roto-translational	(Karman et al., 2015a)
		1850–3000	301–363	5	Fundamental	(Baranov et al., 2005)
		2000–2698	228–272	5	Fundamental	(Lafferty et al., 1996)
		4300–5000	200–330	14	1st overtone	(Hartmann et al., 2017)
	Alternate	30–300	78–129	4	Roto-translational	(Sung et al., 2016)
$O_2 - O_2$	Main	1150–1950	193–353	15	Fundamental	(Baranov et al., 2004)
		7450–8491	296	1	$a^1\Delta_g \leftarrow X^3\Sigma_g^-(0,0)$	(Maté et al., 1999)
		9091–9596	293	1	$a^1\Delta_g \leftarrow X^3\Sigma_g^-(1,0)$	(Karman et al., 2018)
		10,512–11,228	293	1	$a^1\Delta_g \leftarrow X^3\Sigma_g^-(2,0)$	(Spiering and van der Zande, 2012)
		12,600–13,839	296	1	$b^1\Sigma_g^+ \leftarrow X^3\Sigma_g^-(0,0)$	(Tran et al., 2006)
		14,206–14,898	293	1	$b^1\Sigma_g^+ \leftarrow X^3\Sigma_g^-(1,0)$	(Spiering et al., 2011)
		15,290–16,664	203–287	4	Double transitions*	(Thalman and Volkamer, 2013)
		16,700–29,800	203–293	5	Double transitions*	(Thalman and Volkamer, 2013)
	Alternate	7583–8183	206–346	15	$a^1\Delta_g \leftarrow X^3\Sigma_g^-(0,0)$	(Karman et al., 2018)
		9060–9960	206–346	15	$a^1\Delta_g \leftarrow X^3\Sigma_g^-(1,0)$	(Karman et al., 2018)
		10,525–11,125	206–346	15	$a^1\Delta_g \leftarrow X^3\Sigma_g^-(2,0)$	(Karman et al., 2018)
		12,804–13,402	206–346	15	$b^1\Sigma_g^+ \leftarrow X^3\Sigma_g^-(0,0)$	(Karman et al., 2018)
		14,296–14,806	206–346	15	$b^1\Sigma_g^+ \leftarrow X^3\Sigma_g^-(1,0)$	(Karman et al., 2018)
$O_2 - N_2$	Main	1850–3000	301–363	5	N_2 fundamental	(Baranov et al., 2005; Menoux et al., 1993)
		2000–2698	228–272	5	N_2 fundamental	(Lafferty et al., 1996; Menoux et al., 1993)
		7450–8488	293	1	$a^1\Delta_g \leftarrow X^3\Sigma_g^-(0,0)$	(Maté et al., 1999)
		12,600–13,840	296	1	$b^1\Sigma_g^+ \leftarrow X^3\Sigma_g^-(0,0)$	(Tran et al., 2006)
	Alternate	7583–8183	206–346	15	$a^1\Delta_g \leftarrow X^3\Sigma_g^-(0,0)$	(Karman et al., 2018)
		12,804–13,402	206–346	15	$b^1\Sigma_g^+ \leftarrow X^3\Sigma_g^-(0,0)$	(Karman et al., 2018)
N_2-Air	Main	1850–3000	301–363	5	N_2 fundamental	(Baranov et al., 2005; Menoux et al., 1993)
		2000–2698	228–272	5	N_2 fundamental	(Lafferty et al., 1996; Menoux et al., 1993)
		4300–5000	200–330	14	N_2 first overtone	(Hartmann et al., 2017)
O_2-Air	Main	7450–8480	250–296	3	$a^1\Delta_g \leftarrow X^3\Sigma_g^-(0,0)$	(Maté et al., 1999)
		9091–9596	293	1	$a^1\Delta_g \leftarrow X^3\Sigma_g^-(1,0)$	(Karman et al., 2018)
		10,512–11,228	293	1	$a^1\Delta_g \leftarrow X^3\Sigma_g^-(2,0)$	(Spiering and van der Zande, 2012)
		12,600–13,839	300	1	$b^1\Sigma_g^+ \leftarrow X^3\Sigma_g^-(0,0)$	(Tran et al., 2006)
	Alternate	12,990–13,220	298	1	$b^1\Sigma_g^+ \leftarrow X^3\Sigma_g^-(0,0)$	(Drouin et al., 2017)
		7583–8183	206–346	15	$a^1\Delta_g \leftarrow X^3\Sigma_g^-(0,0)$	(Karman et al., 2018)
		9060–9960	206–346	15	$a^1\Delta_g \leftarrow X^3\Sigma_g^-(1,0)$	(Karman et al., 2018)
		10,525–11,125	206–346	15	$a^1\Delta_g \leftarrow X^3\Sigma_g^-(2,0)$	(Karman et al., 2018)
		121,804–13,402	206–346	15	$b^1\Sigma_g^+ \leftarrow X^3\Sigma_g^-(0,0)$	(Karman et al., 2018)
		14,296–14,806	206–346	15	$b^1\Sigma_g^+ \leftarrow X^3\Sigma_g^-(1,0)$	(Karman et al., 2018)
$N_2 - H_2O$	Main	1930–2830	250–350	11	N_2 fundamental	(Hartmann et al., 2018b)
$N_2 - CH_4$	Alternate	0–1379	40–400	10	Roto-translational	(Borysow and Tang, 1993)
$O_2 - CO_2$	Main	12,600–13,839	200–300	1	$b^1\Sigma_g^+ \leftarrow X^3\Sigma_g^-(0,0)$	(Vangvichith et al., 2009)

and B, the binary contributions take the form

$$k(\nu) = k^{(A-A)}(\nu)\,\rho_A^2 + k^{(A-B)}(\nu)\,\rho_A\rho_B + k^{(B-B)}(\nu)\,\rho_B^2, \quad (4)$$

where ρ_A and ρ_B are the number densities of both molecular species. The current updated version of the HITRAN CIA database consistently tabulates binary CIA absorption coefficients $k^{(A-A)}(\nu)$, $k^{(A-B)}(\nu)$, and $k^{(B-B)}(\nu)$, separately. By contrast, the previous version of the database also listed coefficients for different mixtures which had to be scaled

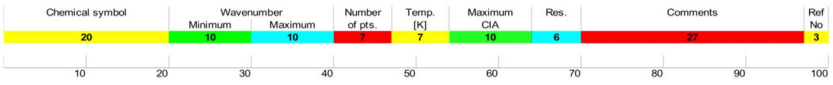

Fig. 2. Definition of the HITRAN CIA header. The numbers indicate the length of each block. Reference numbers identify the sources of the data, which are tabulated in a file available online from www.hitran.org/cia.

with the square of the *total* number density $(\rho_A + \rho_B)^2$. This may have been confusing, and lead to deviations from Eq. (4)–especially when combined with interpolation or extrapolation schemes–and it was inconsistent with the tabulation of theoretical results which obtain $k^{(A-A)}(\nu)$, $k^{(A-B)}(\nu)$, or $k^{(B-B)}(\nu)$ directly, without using mixtures. Fortunately, the only system for which results with different mixtures were previously reported was $O_2 - N_2$. This issue has been fixed in the HITRAN2016 update (Gordon et al., 2017).

Also introduced in the HITRAN2016 update was the concept of an $M -$ Air CIA section, which aims to combine $M - O_2$, $M - N_2$, and $M -$ Ar as ready-to-use absorption coefficients for applications for the Earth's atmosphere. To be explicit,

$$-\frac{ln\,[T(\nu)]}{L} = k^{(M-\mathrm{Air})}(\nu)\,\rho_M \rho_{\mathrm{Air}}, \tag{5}$$

with $\rho_{\mathrm{Air}} = \rho_{O2} + \rho_{N2}$. The $M -$ Air data typically come from three sources:

1. The data may contain the sum of $M - O_2$, $M - N_2$, and $M -$ Ar contributions, where these are separately available. These data should be consistent and hence preferably from the same source, which may be either experimental or obtained from calculations.
2. In many cases the 1% $M -$ Ar data will be unavailable. In these cases, we typically provide 21:79 or 22:78 mixtures of $M - O_2$:$M - N_2$ contributions, depending on whether O_2 or N_2 is to be considered the better model for Ar, which may depend on the transition considered, see Sections 3.4 and 3.7.
3. The data provided as $M -$ Air may also directly come from experiments using either air or a similar mixture, *e.g.* synthetic air.

In summary: where available, the $M -$ Air CIA section gives the recommended binary absorption coefficient. Users should not double count contributions by explicitly adding the contributions of $M - O_2$, $M - N_2$ or $M -$ Ar, which are already accounted for.

3. Data

3.1. $N_2 - N_2$ roto-translational

3.1.1. Main folder

We updated the Main folder $N_2 - N_2$ roto-translational spectrum with the theoretical spectra of Karman et al. (2015a). This replaces the older calculations by Borysow (Borysow and Frommhold, 1986c Borysow, n.d.). In more recent work (Karman et al., 2015a), quantum mechanical line shape calculations were performed, including anisotropic interactions, in the helicity-decoupling or coupled-states approximation. The coupled-states approximation was tested explicitly against coupled-channels calculations at low collision energies, and differences were found only in the region of scattering resonances for very low energies. At higher energies, the results of the calculations including anisotropy were found to approach the isotropic interaction approximation, which is usually invoked in quantum line-shape calculations. This validates that the isotropic approximation is reasonable at high temperature. The effect of interaction anisotropy is to increase the intensity at low temperature, leading to a predicted increase of approximately 20% at $T = 78$ K for $N_2 - N_2$. This effect is consistent with estimates made in Karman et al. (2018), based on a classical statistical mechanical method using the same potential and dipole surface. Recent experiments, as discussed in Section 3.1.2 below, suggest that the effect could be even larger.

3.1.2. Alternate folder

In the Alternate folder, we include new low temperature measurements of the $N_2 - N_2$ roto-translational band (Sung et al., 2016). These are presently unpublished results, and a description of this experiment is given here, awaiting a dedicated publication.

The translation-rotation spectrum of nitrogen gas, from 30 to 300 cm^{-1}, between the temperatures of 78 and 130 K, has been measured at the Jet Propulsion Laboratory using a Fourier transform spectrometer (FTS) coupled to a low temperature multiple-reflection absorption cell which has been previously described in detail (Wishnow et al., 1999; Moazzen-Ahmadi et al., 2015).

Measurements were conducted using an absorption pathlength of 52 m, and details of the spectrometer-detector systems have been previously described (Wishnow et al., 1999; Moazzen-Ahmadi et al., 2015). Background spectra were obtained interspersed between N_2 spectra, with the cell filled with He gas at pressures and temperatures close to those of the N_2 samples so that effects in the spectra due to window distortion, mirror alignment, or mirror reflectivity were minimized. The N_2 and He gases used had stated purities of 99.999%, and gas pressures were between 0.6 and 2.5 atm. Spectra typically comprised an average about 72 interferograms, at a spectral resolution of 0.15 cm^{-1}, requiring about 20–30 min of data collection.

Fig. 3 shows representative absorption coefficient spectra (absorbance divided by density squared) at four temperatures. At each temperature the estimated error is 3% of the peak of the curve. In the 78 K spectrum, this appears as a systematic non-zero offset that is observed at 250 cm^{-1}. The solid curves are the new measurements, the red dot-dash curves denote Borysow model spectra (Borysow and Frommhold, 1986c Borysow, n.d.), and the diamonds indicate results from the Karman calculation, (Karman et al., 2015a) which is provided in the HITRAN Main folder as described above, in Section 3.1.1. The 78 K graph also shows a magenta curve denoting a previous low-wavenumber spectrum obtained with this cell, but with a different spectrometer system (Wishnow et al., 1996), where these measurements have an error of ± 5% in the absorption. These previous measurements are 7% greater at the peak than the current measurements, but this difference is not significant given their uncertainties. Gaps in the spectra arise from wavenumber regions where acoustic resonances cause prominent spikes. The ripples in the spectra with an ~8 cm^{-1} period are attributed to blended N_2-N_2 dimer transitions, examined previously (Wishnow et al., 1996). At each temperature, the measurements show stronger absorption than is predicted by the models. For the temperatures 78.3, 89.3, 109.6, and 129.0 K, the measurements at the peak exceed the Borysow models by 19, 14, 10, and 8%, respectively. The data in Dagg et al. (1985) at 126 K with experimental errors of ± 10% are lower than the present values at 129.0 K by 9%. Further details of these measurements and the temperature variation of the deviations from the models will be discussed in a forthcoming paper.

3.2. N_2 fundamental in $N_2 - N_2$, $N_2 - O_2$ and $N_2 -$ Air

In the Richard et al. (2012) effort, the fundamental band $N_2 - N_2$ data were provided based on data from Baranov et al. (2005) and Lafferty et al. (1996). It is worth mentioning that the data from Lafferty et al. (1996) corresponding to $T = 243.15$ K had a reduced amount of significant figures resulting in the somewhat jagged appearance of the spectrum. One should also note that the dataset corresponding to $T = 233$ K seems to disagree with the observations carried out with the ACE-FTS satellite measurements (Sioris et al., 2014). Lafferty et al. (1996) proposed an empirical expression allowing one to calculate the

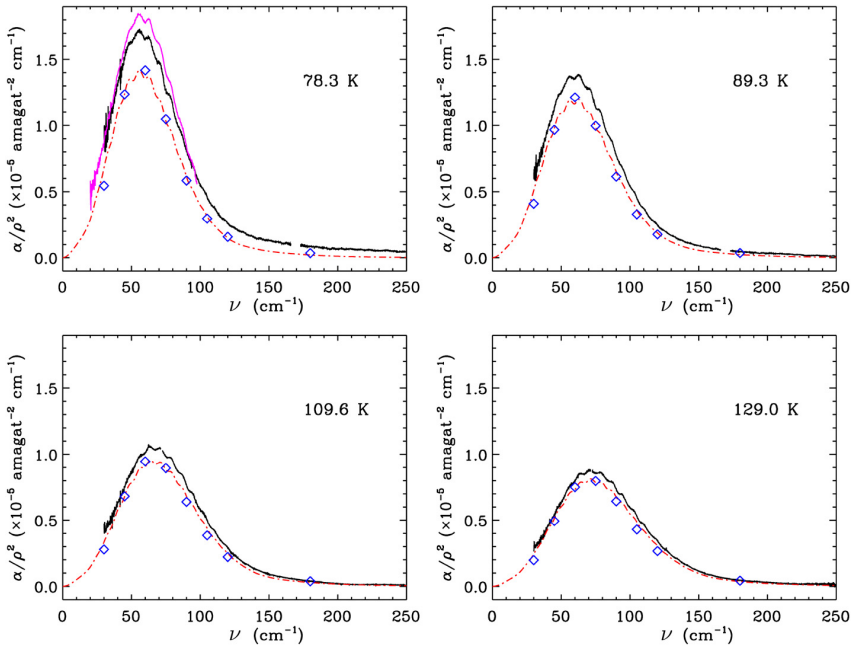

Fig. 3. $N_2 - N_2$ collision-induced absorption spectra at four temperatures. The solid black curves are the newly included low-temperature measurements, the red dot-dash curves denote Borysow model spectra (Borysow, n.d.), and the blue diamonds show Karman model results interpolated to the specified temperatures (Karman et al., 2015a). The magenta curve in the 78 K graph shows previous measurements using the same absorption cell, but with a different spectrometer system (Wishnow et al., 1996).

$N_2 - N_2$ absorption (see Eq. (4) and Table 1 of that paper) at different temperatures (within the range encountered in the terrestrial atmosphere). Sioris et al. (2014) have noted some differences between the values calculated using that expression and experimental data from Lafferty et al. (1996) and Menoux et al. (1993), and proposed slight modifications to the coefficients reported in Table 1 of Lafferty et al. and also extended the wavenumber range from $\leq 2600\,cm^{-1}$ to $\leq 2640\,cm^{-1}$.

In the previous effort, no $N_2 - O_2$ values were provided in the region of the N_2 fundamental. However, Menoux et al. (1993) reported that $N_2 - O_2$ and $N_2 - N_2$ absorption have identical shapes through the entire band, and that one can calculate the $N_2 - O_2$ CIA by scaling the $N_2 - N_2$ absorption. Lafferty et al. (1996) used the data from Menoux et al. (1993) to determine an empirical scaling expression [Eq. (7) of Lafferty et al., 1996] describing the temperature dependence of the ratio of $N_2 - O_2$ and $N_2 - N_2$ absorption. This expression was used in this work to calculate the $N_2 - O_2$ CIA in addition to the existing $N_2 - N_2$ values. Moreover, assuming 21:79 mixture of $M - O_2$:$M - N_2$ contributions to the $N_2 -$ Air values are also provided.

3.3. $N_2 - N_2$ first overtone

The $N_2 - N_2$ CIA data, which already contained the roto-translational and fundamental bands in HITRAN, was extended to include the first overtone region, near 2.16 μm. In this region, two processes contribute to the absorption: Either one of the two colliding molecules can make the $v = 2 \leftarrow 0$ transition,

$$N_2(v = 2) + N_2(v = 0) \leftarrow N_2(v = 0) + N_2(v = 0), \quad (6)$$

or alternatively, *double transitions* can occur in which both molecules make v $=1\leftarrow 0$ transitions,

$$N_2(v = 1) + N_2(v = 1) \leftarrow N_2(v = 0) + N_2(v = 0). \quad (7)$$

These processes lead to overlapping spectra which are not resolved individually, but their sum is observable in atmospheric spectra. The HITRAN line-by-line section also contains electric quadrupole transitions in this region.

Unlike in the fundamental region, the collision-induced band near the first overtone has not been measured extensively and only two papers at room temperature (Shapiro and Gush, 1966) and at 97.5 K (McKellar, 1989) exist. Up to this time atmospheric scientists have chosen to ignore this contribution or digitize room temperature plots from the 1966 work of Shapiro and Gush (1966).

Due to the lack of experimental data, the included $N_2 - N_2$ first-overtone CIA spectra have been calculated by Hartmann et al. (2017) using classical molecular dynamics simulations (CMDS). In these calculations, an ensemble of 10^6 molecules has been simulated at constant temperature and number density. The auto-correlation function of the transition dipole moment has been obtained from these simulations, and its Fourier transform is computed to yield the absorption spectrum. The force field describing the $N_2 - N_2$ interactions is taken from Bouanich (1992), which uses site-site Lennard-Jones and Coulomb interactions. The transition dipole moment is estimated from long-range theory, using known multipole moments and polarizabilities of N_2. The obtained spectra have been corrected by an empirical temperature-dependent scaling factor and wavenumber shift.

HITRAN CIA tabulates spectra for $N_2 - N_2$ at 14 temperatures between 200 and 330 K, which are also covered in the roto-translational and fundamental bands. These have been obtained from an interpolation scheme, Eq. (3) of Hartmann et al. (2017). The absorption by $N_2 - N_2$ at 300 K is shown in Fig. 4, together with the roto-translational and fundamental bands.

3.4. $N_2 -$ Air first overtone

The collision-induced band near the first overtone of N_2 is also provided for air mixtures, as determined from the semiempirically-corrected CMDS calculations in Hartmann et al. (2017). In addition to the $N_2 - N_2$ contribution discussed above, this includes an estimate of the $N_2 - O_2$ contribution to the CIA in this band. The $N_2 - O_2$ contribution is obtained from similar CMDS calculations, where the dipole moment surface is again estimated from molecular multipole moments and polarizabilities, and the $N_2 - O_2$ interaction potential is estimated from models of the $N_2 - N_2$ and $O_2 - O_2$ potentials.

The air mixture used in the calculations is 22% O_2, and 78% N_2, as O_2 is considered to be an appropriate model for the missing 1% argon: Argon, like O_2 but unlike N_2, does not contribute through double transitions.

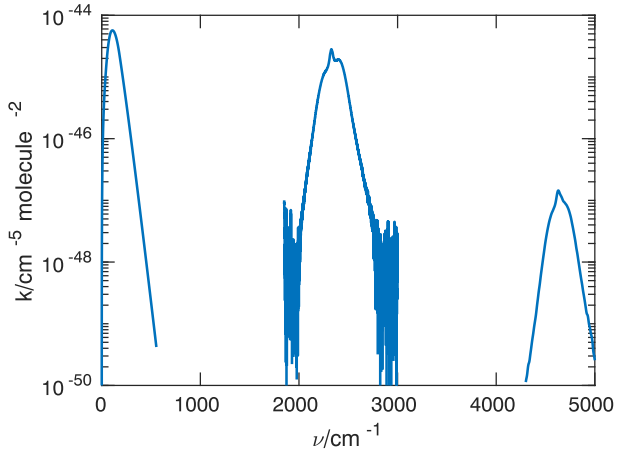

Fig. 4. Semi-logarithmic plot with roto-translational, fundamental and first overtone bands of $\mathbf{N_2 - N_2}$ at $\boldsymbol{T = 300}$ K. Data shown for these three bands are those contained in the Main folder, which are originally from Karman et al. (2015a), Baranov et al. (2005), and Hartmann et al. (2017), respectively.

As shown in Hartmann et al. (2017), these spectra can be applied to determine the baseline in atmospheric spectra near 2.16 μm. As a consistency check, it is shown that the correct known atmospheric N_2 mole fractions are retrieved. The effects of including the $N_2 - Air$ CIA from these new data, rather than by fitting the curvature of the background, on the retrieval of other molecules were also discussed (Hartmann et al., 2017).

3.5. Newly added $O_2 - O_2$ $a^1\Delta_g \leftarrow X^3\Sigma_g^-(2,0)$ and $b^1\Sigma_g^+(1,0)$ bands

Collision-induced absorption for various electronic transitions of O_2 are already included in HITRAN. Here, the set is extended with the $a^1\Delta_g \leftarrow X^3\Sigma_g^-(2,0)$ and $b^1\Sigma_g^+ \leftarrow X^3\Sigma_g^-(1,0)$ bands from Spiering and van der Zande (2012) and Spiering et al. (2011), respectively. In both cases, these are obtained from cavity ring-down spectroscopy experiments. Measurements were performed using pressure ramps, where the density was increased up to 5–7 amagat. The collision-induced contribution was determined by fitting a quadratic pressure dependence, after removing monomer absorption, including line mixing (which was not needed for $v = 2$) and Rayleigh scattering.

The experimental data contain considerable scatter and, in order to provide smooth spectra for the database, we performed a fit to the simple line-shape function

$$L(\nu) = \begin{cases} S\dfrac{\Gamma}{\Gamma^2 + (\nu - \nu_0)^2} & \text{for } \nu \geq \nu_0. \\ S\exp\left[\dfrac{\hbar(\nu - \nu_0)}{k_B T}\right]\dfrac{\Gamma}{\Gamma^2 + (\nu - \nu_0)^2} & \text{for } \nu < \nu_0. \end{cases} \quad (8)$$

This line-shape function corresponds to a Lorentzian in the blue wing, whereas the red wing is weaker by a Boltzmann factor, in accordance with an approximate detailed balance relation derived in Karman et al. (2018). The fit parameters S, Γ, and ν_0 determine the intensity, width, and position of the Lorentzian blue wing, whereas the asymmetry of the profile is determined by the thermal energy, k_BT, without adjustable parameters. The resulting fits are shown in Fig. 6, and essentially reproduce the experimental data to within their scatter or error bars.

Collision-induced absorption for all $O_2 - O_2$ bands included in HITRAN is shown in Fig. 5.

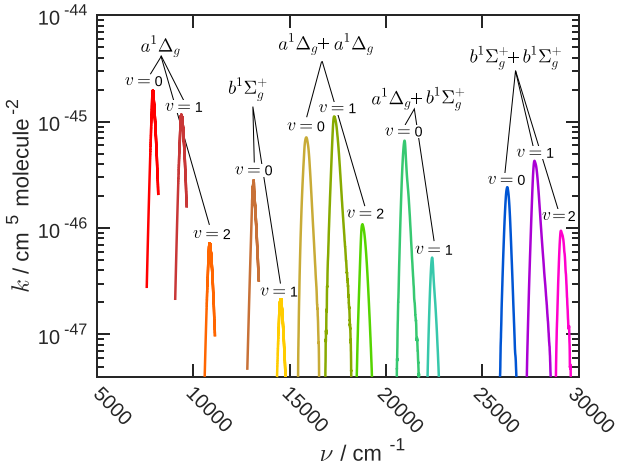

Fig. 5. Overview of all $\mathbf{O_2 - O_2}$ electronic transitions included in this work. Transitions marked $\boldsymbol{a^1\Delta_g}$ and $\boldsymbol{b^1\Sigma_g^+}$ represent single transitions to these electronic states from the $\boldsymbol{X^3\Sigma_g^-}$ ground state, where the collision partner is not excited electronically. Bands labeled $\boldsymbol{a^1\Delta_g + a^1\Delta_g}$, $\boldsymbol{a^1\Delta_g + b^1\Sigma_g^+}$ and $\boldsymbol{b^1\Sigma_g^+ + b^1\Sigma_g^+}$ are double electronic transitions, where both colliding molecules are excited electronically. Vibrational structure is resolved as is indicated. We note that vibrational excitations that occur in both colliding molecules – including those not excited electronically – are not resolved individually, and contribute to the same vibronic bands.

3.6. Updated $O_2 - O_2/N_2/Air$ $a^1\Delta_g \leftarrow X^3\Sigma_g^-(1,0)$ and $b^1\Sigma_g^+(0,0)$ bands

The $O_2 - O_2$ $a^1\Delta_g \leftarrow X^3\Sigma_g^-(1,0)$ band was updated with cavity ring-down experimental data on $O_2 - O_2$ and $O_2 - N_2$ from Karman et al. (2018), similar to those described in Section 3.5. This update replaced the data of Greenblatt et al. (1990).

The Alternate folder contains the $O_2 - Air$ $b^1\Sigma_g^+ \leftarrow X^3\Sigma_g^-(0,0)$ data of Drouin et al. (2017). These spectra have been obtained in a multi-spectrum fitting approach that was fitted to laboratory data in the P-branch, but with CIA extracted from the total carbon column observing network (TCCON) atmospheric data for the R-branch (Wunch et al., 2011a). When used together with the speed-dependent Voigt (SDV) monomer line list available in HITRAN, these data reduce systematic biases between remote sensing and validation measurements. The results previously available from Tran et al. (2006) are still available in the Main folders for $O_2 - O_2$, $O_2 - N_2$, and $O_2 - Air$. These spectra are significantly broader and less structured, and seem to be in better agreement with the theoretical study of Karman et al. (2018), the data of which are available in the Alternate folders and discussed in Section 3.7. The differences are discussed in Karman et al. (2018). Further experimental studies are needed to address this issue.

We stress that the $O_2 - Air$ $b^1\Sigma_g^+ \leftarrow X^3\Sigma_g^-(0,0)$ A-band contained in the *Alternate* folder is *recommended* for use together with the SDV monomer line list from HITRAN2016 (Gordon et al., 2017). The $O_2 - Air$ data in the Main folder is consistent with the $O_2 - O_2/N_2$ data and matches closely with independent theoretical results, but leads to larger systematic biases in atmospheric retrievals.

3.7. $O_2 - O_2/N_2/Air$ $a^1\Delta_g$, $b^1\Sigma_g^+ \leftarrow X^3\Sigma_g^-$ temperature dependence

Here, we include the theoretical temperature dependence of the $a^1\Delta_g \leftarrow X^3\Sigma_g^-(0-2,0)$ and $b^1\Sigma_g^+ \leftarrow X^3\Sigma_g^-(0-1,0)$ bands from Karman et al. (2018). For these transitions, experimental data are typically available for a single temperature, or a limited set of temperatures in a range where the temperature dependence is weak. Temperature extrapolation is provided in the relevant Alternate folders where the estimates are formed as follows: Absorption spectra were

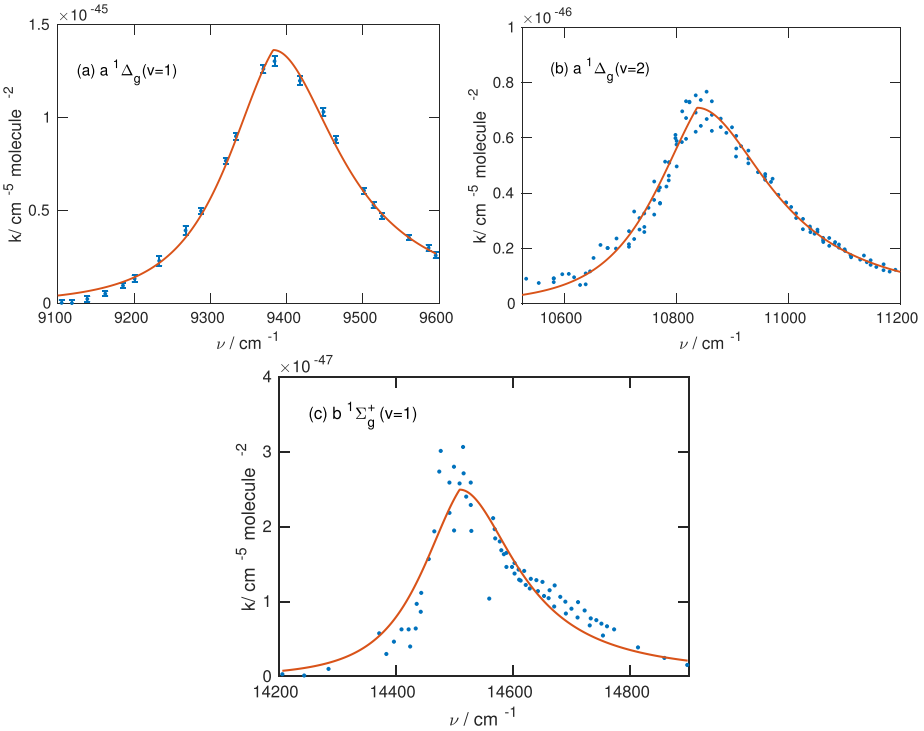

Fig. 6. Panels (a), (b), and (c) show the experimental data and modified Lorentzian fit thereto, included in HITRAN, for the $a^1\Delta_g \leftarrow X^3\Sigma_g^-(1,0)$, $(2,0)$, and $b^1\Sigma_g^+ \leftarrow X^3\Sigma_g^-(1,0)$ bands, respectively.

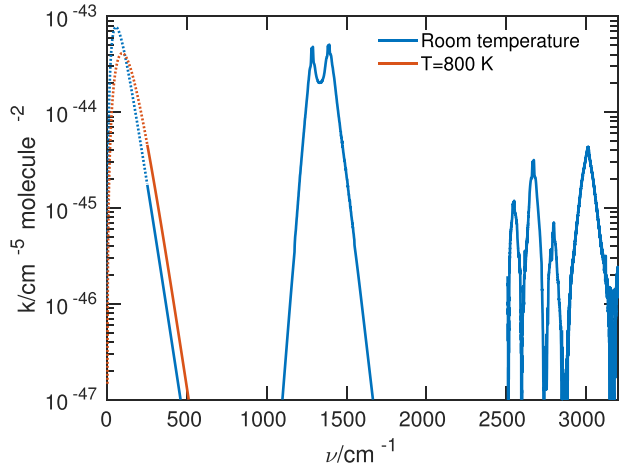

Fig. 7. Roto-translational, $\nu_1/2\nu_2$, $2(\nu_1/2\nu_2)$, and $\nu_2+\nu_3$ bands of CO_2-CO_2 at $T = 313$ K and $T = 800$ K. The dotted part of the lines denotes the region $\nu < 250\ cm^{-1}$, which was already available in HITRAN (Richard et al., 2012). Data for the four bands shown are from Gruszka and Borysow (1997), Baranov and Vigasin (1999), Baranov et al. (2003a), and Baranov (2018), respectively.

calculated in the isotropic interaction approximation for temperatures between 78 K and 400 K, and subsequently corrected for interaction anisotropy using a statistical mechanical model. These spectra were subsequently scaled by an overall, temperature-independent factor, which was determined by fitting to the experimental data at the available temperature.

The above estimates are also given for the vibrational transitions, where experimental data are available, although the model calculations do not explicitly include the vibrational coordinates.

Estimates are similarly given for O_2-N_2. In this case, only the relevant "spin-orbit" mechanism contributes (Karman et al., 2018), and the N_2 polarizability is used to compute the model transition dipole moment. Otherwise, the calculation is unchanged from the O_2-O_2 system. Data for O_2-Air is estimated as 21% O_2-O_2 and 79% O_2-N_2. Nitrogen is considered a reasonable model for the missing 1% Argon, which is diamagnetic, like N_2.

3.8. O_2-O_2 double electronic transitions

The experimental spectra for the O_2-O_2 double electronic transitions between 630 and 344 nm were updated (Thalman and Volkamer, 2013). The observed bands correspond to transitions where both molecules are initially in the electronic and vibrational ground state, $X^3\Sigma_g^- + X^3\Sigma_g^-$, to excited states of the complex where both molecules are excited electronically, $a^1\Delta_g + a^1\Delta_g$ ($\nu = 0,\ 1,\ 2$), $a^1\Delta_g + b^1\Sigma_g^+$ ($\nu = 0,\ 1$), and $b^1\Sigma_g^+ + b^1\Sigma_g^+$ ($\nu = 0,\ 1,\ 2$). In this notation, by ν we denote the total quanta of vibrational excitation in the complex. For example, the $a^1\Delta_g + a^1\Delta_g$ $(2,0)$ band has contributions from the following vibronic transitions,

$$\begin{aligned}
&O_2(\alpha^1\Delta_g v=2) + O_2(\alpha^1\Delta_g, v=0) \leftarrow O_2(X^3\Sigma_g^-, v=0) + O_2(X^3\Sigma_g^-, v=0)\\
&O_2(\alpha^1\Delta_g v=1) + O_2(\alpha^1\Delta_g, v=1) \leftarrow O_2(X^3\Sigma_g^-, v=0) + O_2(X^3\Sigma_g^-, v=0)\\
&O_2(\alpha^1\Delta_g v=0) + O_2(\alpha^1\Delta_g, v=2) \leftarrow O_2(X^3\Sigma_g^-, v=0) + O_2(X^3\Sigma_g^-, v=0)
\end{aligned} \tag{9}$$

and the $a^1\Delta_g + b^1\Sigma_g^+$ $(1,0)$ band consists of

$$\begin{aligned}
&O_2(\alpha^1\Delta_g v=1) + O_2(b^1\Sigma_g^+, v=0) \leftarrow O_2(X^3\Sigma_g^-, v=0) + O_2(X^3\Sigma_g^-, v=0)\\
&O_2(\alpha^1\Delta_g v=0) + O_2(b^1\Sigma_g^+, v=1) \leftarrow O_2(X^3\Sigma_g^-, v=0) + O_2(X^3\Sigma_g^-, v=0)\\
&O_2(b^1\Sigma_g^+ v=1) + O_2(a^1\Delta_g, v=0) \leftarrow O_2(X^3\Sigma_g^-, v=0) + O_2(X^3\Sigma_g^-, v=0)\\
&O_2(b^1\Sigma_g^+ v=0) + O_2(a^1\Delta_g, v=1) \leftarrow O_2(X^3\Sigma_g^-, v=0) + O_2(X^3\Sigma_g^-, v=0)
\end{aligned} \tag{10}$$

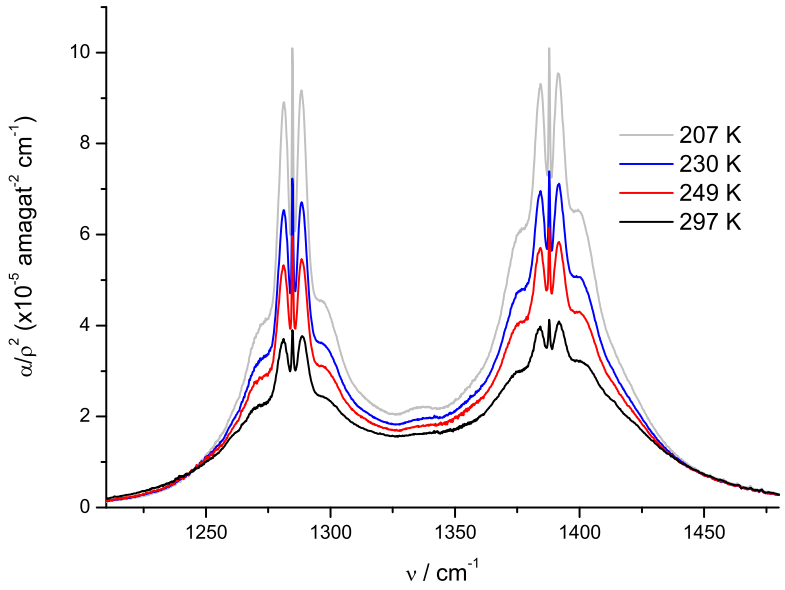

Fig. 8. CIA spectra of the $CO_2 - CO_2$ Fermi dyad at 207, 230, 249, and 297 K based on Baranov and Vigasin (1999) and Baranov et al. (2004).

Interestingly, the intensities for these simultaneous transitions in this region do not follow Franck-Condon factors at all. The (1, 0) vibrational transitions for the $a^1\Delta_g + a^1\Delta_g$ and $b^1\Sigma_g^+ + b^1\Sigma_g^+$ electronic transitions are even observed to be stronger than the (0, 0) bands. There is no theoretical prediction of these intensities, except for the qualitative argument that the exchange-induced transition dipole moment may be strongly dependent on the vibrational coordinate, such that one may expect the scaling with Franck-Condon factors to break down completely (Karman et al., 2018). This is in agreement with the $a^1\Delta_g(v > 0)$ and $b^1\Sigma_g^+(v > 0)$ single transitions, which in $O_2 - O_2$ are observed and are stronger than expected on the basis of Franck-Condon factors, whereas the $O_2 - N_2$ transitions–which are not driven by exchange–are weak and not observed (Karman et al., 2018).

For all double transition bands, an increase in the peak absorption cross-section at lower temperatures corresponds to a narrowing of the spectral band width, which is relatively more pronounced at temperatures below 253 K. The integrated cross-section remains constant for temperatures between 203 and 293 K (Thalman and Volkamer, 2013). This temperature effect has been confirmed by field observations of $O_2 - O_2$ near 477 nm in limb spectra in a cold Rayleigh atmosphere, and in direct-sun DOAS measurements from the ground (Spinei et al., 2015). Bound O_4 dimer absorption had been observed in molecular beam experiments; however it appears that at the temperatures accessible in the Earth atmosphere $O_2 - O_2$ absorption can essentially be explained by CIA (Thalman and Volkamer, 2013).

Further laboratory work is needed to better decouple absorption by $O_2 - O_2$ CIA from overlapping absorption by the gamma band of O_2 near 630 nm. Furthermore, $O_2 - O_2$ absorption bands of the $a^1\Delta_g + b^1\Sigma_g^+$ ($v = 2$) and $b^1\Sigma_g^+ + b^1\Sigma_g^+$ ($v = 3$) transitions have been observed in atmospheric spectra around 419 nm and 328 nm (Lampel

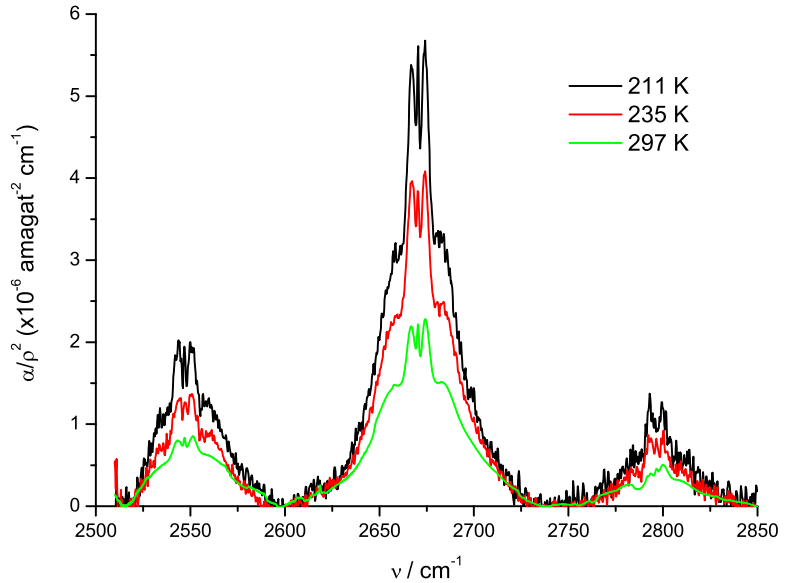

Fig. 9. CIA spectra of the Fermi triad at $T = 211$, 235, and 297 K (Baranov et al., 2003a).

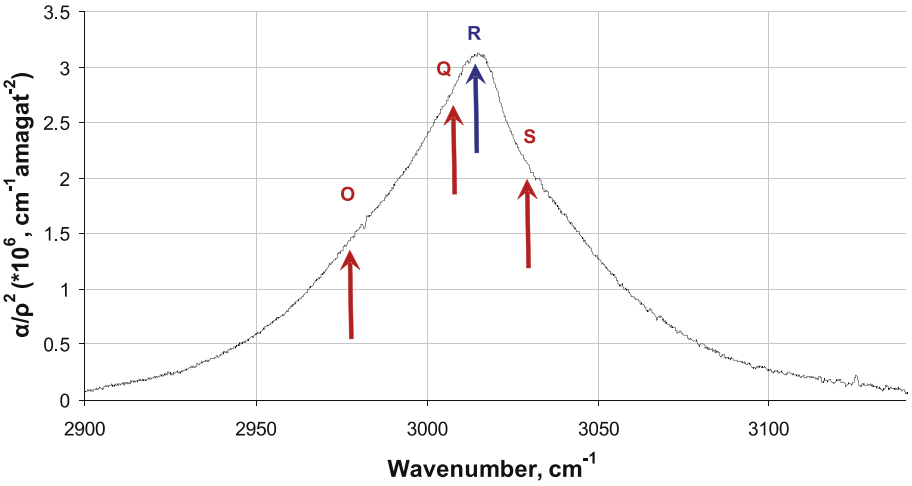

Fig. 10. The measured $\nu_2 + \nu_3$ CIA band profile (Baranov, 2018). Red arrows show the location of strongest transitions (at 294.8 K) of O–, Q–, and S–branches corresponding to conventional CIA selection rules $\Delta J = 0, \pm 2$. The blue arrow indicates the strongest transition of the R–branch ($\Delta J = 1$), the position of which matches surprisingly closely with the observed band maximum. (For interpretation of the references to color in this figure legend, the reader is referred to the web version of this article.)

et al., 2018). There are currently no gas-phase laboratory spectra of these bands. Despite the weakness of these bands, they potentially still interfere with atmospheric remote sensing of trace gases.

HITRAN now includes the spectra for the double electronic transitions recorded by Thalman and Volkamer (2013). This replaces the previous data by Hermans (n.d.). The new data set agrees to within 5% with the old data for the strong bands at room temperature, but also provides data for lower temperatures, down to 200 K. The vibration-electronic bands of $O_2 - O_2$ can be seen in Fig. 5.

3.9. $CO_2 - CO_2$ roto-translational band

The roto-translational band, adapted from Gruszka and Borysow (1997) was revised in the present update. It was shown by Wordsworth et al. (2010), that many atmospheric models are sensitive to absorption in the 250–500 cm^{-1} window, particularly when the atmospheric abundance of H_2O is low, as is the case on Venus and Mars. Therefore, the data of Gruszka and Borysow (1997), which has been calculated only up to 250 cm^{-1}, has been extrapolated assuming exponential decay of the wings. Especially for the higher temperatures, there is substantial absorption beyond 250 cm^{-1}. This is illustrated in Fig. 7.

The nominal temperature range for which the roto-translational band was simulated in Gruszka and Borysow (1997) extends from 200 K to 800 K. It is worth pointing out that the measurements at 200 K, carried out recently at the AILES facility of the SOLEIL synchrotron, (Joalland et al., 2016) revealed a notable departure of observed roto-translational band shape from that calculated in Gruszka and Borysow (1997). Although these measurements require further verification, one has to consider possible increased absorption near the band maximum and diminished absorption in the long-wave wing. This inconsistency between low temperature measurements and calculations from Gruszka and Borysow could be due to the contribution from true bound carbon dioxide dimers, which were largely disregarded in the molecular dynamics simulations of Gruszka and Borysow (1997). Later, more advanced molecular dynamics calculations have been carried out in Hartmann et al. (2011). Here, a significant underestimate of the calculated absorption below 50 cm^{-1} was observed in the low-temperature spectra. Among other effects, the lack of dimer absorption was mentioned in Hartmann et al. (2011) as a possible cause of departure among molecular dynamics simulations and observations.

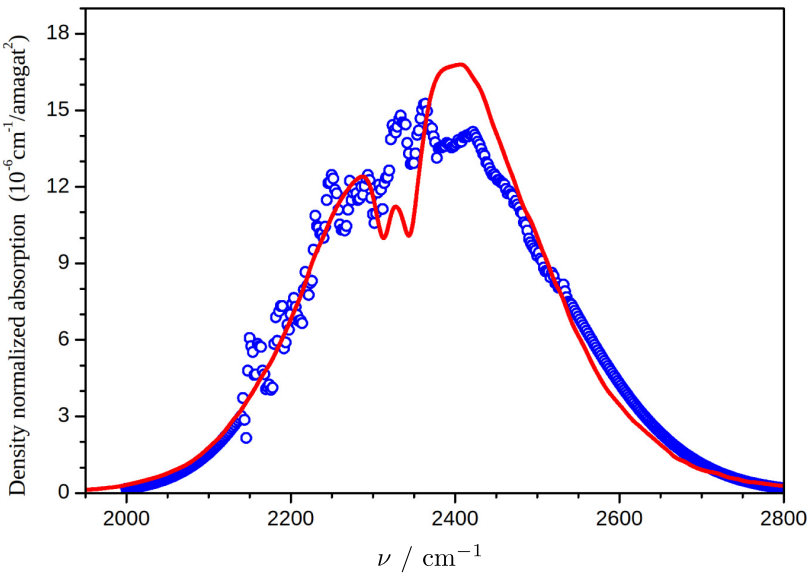

Fig. 11. Comparison between the simulated $N_2 - H_2O$ CIA spectrum of Hartmann et al., 2018b (red line), now included in HITRAN, and the experimental spectrum of Baranov et al., 2012 (blue symbols), both at 352 K. (For interpretation of the references to color in this figure legend, the reader is referred to the web version of this article.)

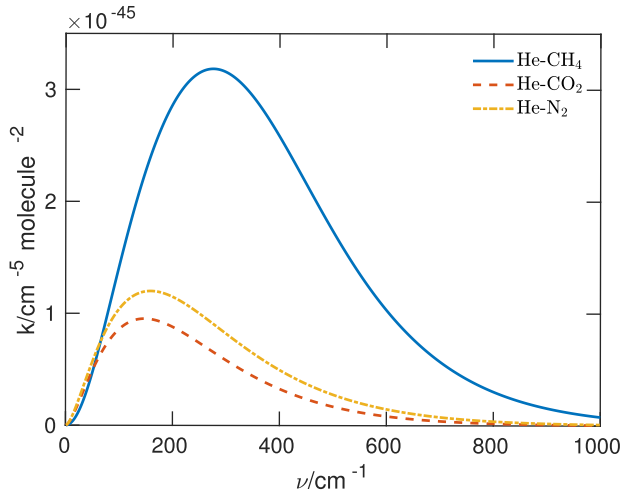

Fig. 12. Comparison of roto-translational bands for different **He**−***X*** collision systems at $T = 300$ K.

3.10. $CO_2 - CO_2$ $\nu_1/2\nu_2$ at 7.5 μm

We extend the $CO_2 - CO_2$ dataset with the measured absorption spectra near the $\nu_1/2\nu_2$ monomer vibrational transitions. These spectra have been measured accurately by Baranov, initially at 291 K and subsequently in the extended temperature range 193–360 K (Baranov et al., 2004).

Fig. 8 shows the binary absorption spectrum after subtraction of minor contamination from water vapor and allowed monomer lines of the less abundant $^{16}O^{12}C^{18}O$ isotopologue. The spectra obtained show sharp and strongly temperature-dependent P,Q,R–structures superimposed on a smoother and broader background of both Fermi coupled components. The positions of the sharpest Q–branches correspond closely to those detected during the coherent anti-Stokes Raman spectroscopy (CARS) probe of $(CO_2)_2$ dimers formed in a supersonic expansion (Huisken et al., 1997). Although they are rotationally unresolved at room temperature, the shape of the structured features seated atop a smoother background indicates that they are due to "centrosymmetric parallelogram structure" van der Waals-bound $CO_2 - CO_2$ dimers (Baranov and Vigasin, 1999; Baranov et al., 2003b).

3.11. $CO_2 - CO_2$ $2(\nu_1/2\nu_2)$ at 3.75 μm

The Fourier transform spectra in the range of the Fermi triad were measured with 0.5 cm^{-1} resolution at $T = 211$, 235, and 297 K using two White type multi-pass cells of 30 m and 84 m optical path lengths (Baranov et al., 2003a). The noise level in the two lower temperature spectra is significantly more pronounced than that in the room temperature spectrum. Nevertheless the presence of true dimer features can be clearly traced even by eye at least in the high-wavenumber componentsof the three coupled CIA bands at pressure as low as near 1 atm. Fig. 9 shows the CIA profile of the Fermi triad after removal of the allowed isotopic bands and the strong wing of the ν_3 CO_2 band.

3.12. $CO_2 - CO_2$ around 3000 cm^{-1}

The IR absorption spectra of pure carbon dioxide in the region of the forbidden $\nu_2 + \nu_3$ vibrational transition at 3004 cm^{-1} have been recorded with a Fourier-transform spectrometer with a multi-pass cell as is described in more detail in Baranov, 2018. The data were taken at 294.8 K with a resolution of 0.02 cm^{-1} over the spectral range 2500 to 3500 cm^{-1}. The measured binary absorption coefficients provide the band integrated intensity value of $(2.39 \pm 0.04) \times 10^{-4}$ cm^{-2} $amagat^{-2}$. The band profile looks like a slightly asymmetric single-maximum bell-shape, see Fig. 10. The spectral shape of this band shows no distinct features that could be attributed to $CO_2 - CO_2$ dimers. This contrasts with the case of the Fermi-coupled dyad (ν_1, $2\nu_2$) and triad $2(\nu_1, 2\nu_2)$ bands where pronounced dimer signatures are observed, see Figs. 8 and 9.

3.13. $CO_2 - H_2$

Collision-induced absorption by $CO_2 - H_2$ complexes makes an important contribution to the climate balance of weakly reducing CO_2-rich atmospheres, and has been suggested to be important for the resolution of the *faint young Sun* problem (Wordsworth et al., 2017). In fact, the $CO_2 - H_2$ CIA may be far more efficient than other contributors, such as $N_2 - N_2$, because the roto-translational band of $CO_2 - H_2$ extends to higher wavenumbers. Importantly, this gives rise to absorption of outgoing radiation in the 250–500 cm^{-1} spectral window of the early Martian atmosphere, near the peak of the blackbody emission spectrum for temperatures in the 250–300 K range (Wordsworth and Pierrehumbert, 2013).

Here, we included the estimate of the $CO_2 - H_2$ CIA spectra as

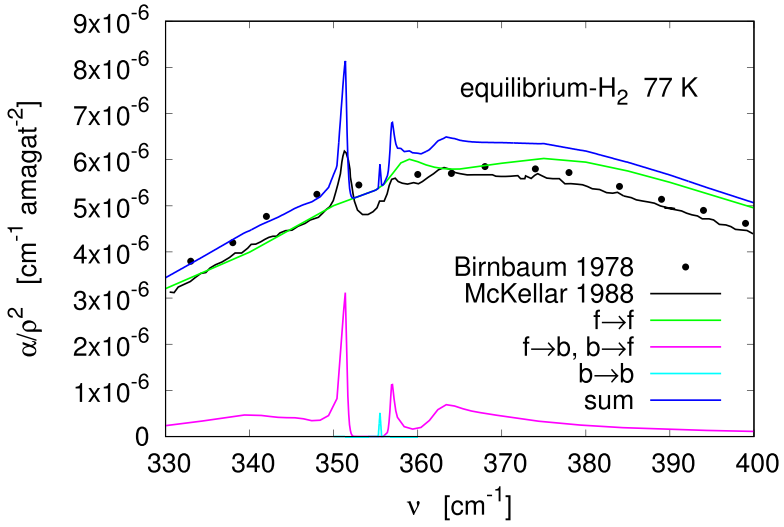

Fig. 13. The absorption coefficient at 77 K, normalized by the square of the hydrogen density, around the S(0) transition in equilibrium-hydrogen. The contributions of transitions between free (f) and bound (b) states are also shown. The laboratory measurement of McKellar (1988) was taken at a number density of 2.63 amagats. Birnbaum's measurement (Birnbaum, 1978) is broad-band and does not resolve the dimer features. It is shown for comparison of the overall magnitude of absorption. Reproduced with permission from Fletcher et al. (2018).

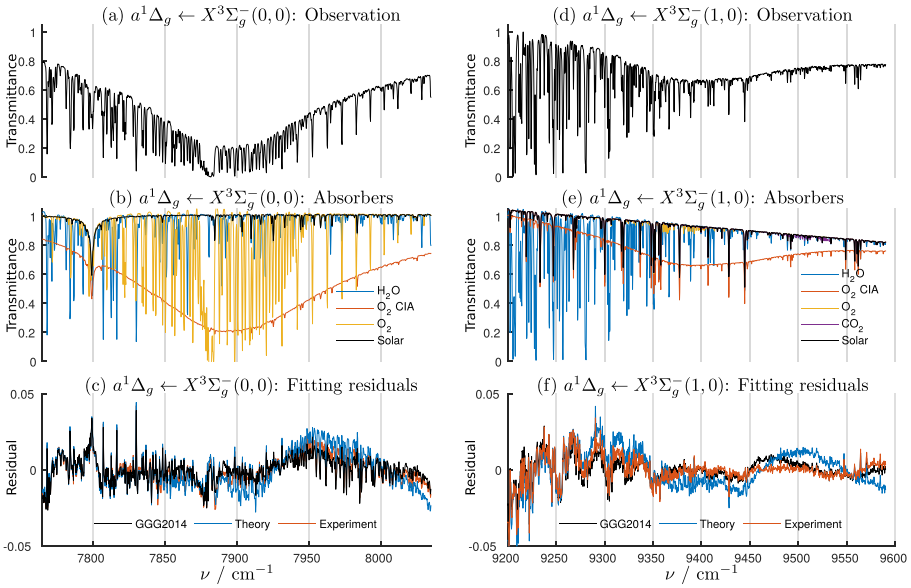

Fig. 14. (a) FTS observation spectrum collected at Cambridge, MA (42.377162 N, −71.113461 W) at 20:07:43 EDT on 24 June 2016 for the $\boldsymbol{a^1\Delta_g \leftarrow X^3\Sigma_g^-(0,0)}$ band. The spectrum is apodized using medium Norton–Beer function. (b) The contributions of different atmospheric absorbers. (c) Fitting residuals of using different CIA spectra. (d-f) the same as (a-c) but for the $\boldsymbol{a^1\Delta_g \leftarrow X^3\Sigma_g^-(1,0)}$ band.

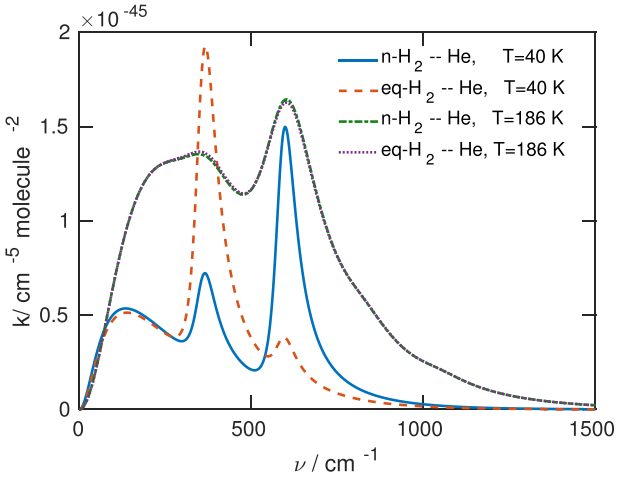

Fig. 15. Roto-translational spectra of $\mathbf{H_2 - He}$ for normal $\mathbf{H_2}$ ($\boldsymbol{n}$ − $\mathbf{H_2}$) and equilibrium $\mathbf{H_2}$ (**eq** − $\mathbf{H_2}$) at $\boldsymbol{T}$ = **40** K and 186 K. This data was already contained in the original release of the HITRAN CIA section, and is taken from Borysow et al. (1988).

modeled by Wordsworth et al., 2017. The model assumes that the spectrum of $CO_2 - H_2$ can be approximated as a linear combination of the spectra of both pure substances, $CO_2 - CO_2$ and $H_2 - H_2$. Binary absorption coefficients for these latter spectra are weighted by two coefficients which were determined based on the zeroth order spectral moments for roto-translational bands of pure gases, as well as the newly calculated zeroth spectral moment for $CO_2 - H_2$ molecular pairs. The zeroth moment characterizes the integrated intensity of the band and can be calculated either in terms of the integral of the binary absorption coefficient over the wavenumbers or using the squared induced dipole integrated over the phase space, see Frommhold, 2006. The zeroth moment was calculated in Wordsworth et al., 2017 in the classical approximation using *ab initio* potential energy and dipole moment surfaces for $CO_2 - H_2$. To check the validity of retrieved spectra, the same procedure was applied to reproduce CIA spectra for the similar system $N_2 - H_2$, for which experimental and calculated band shapes are known. Satisfactory agreement of this test simulation largely supports prediction of the $CO_2 - H_2$ spectrum, although the accuracy of this estimate remains uncertain until more sophisticated methods are used to retrieve the CIA spectral shape for this system.

3.14. $CO_2 - CH_4$

Like $CO_2 - H_2$ discussed in the previous section, $CO_2 - CH_4$ is an efficient absorber of outgoing long-wave radiation relevant to CO_2-rich atmospheres. Also for this collisional pair, no experimental or theoretical line shapes are available, and we included the estimates of the model calculations of Wordsworth et al., 2017. The reader is referred to the previous section, 3.13, for a summary, or to the original research article for a more detailed description (Wordsworth et al., 2017).

3.15. N_2 fundamental in $N_2 - H_2O$

Laboratory measurements of the absorption in the fundamental band of N_2 induced by collision with H_2O have been presented in Baranov et al., 2012. These data were obtained from measurements made for several $N_2 - H_2O$ mixtures with various partial pressures of H_2O complemented with about 4 bars of N_2 (Baranov, 2011). Absorption was studied at four temperatures (326, 339, 352, and 363 K), but due to the relatively large uncertainties, no reliable temperature dependence could be retrieved that would enable extrapolations to lower temperatures, relevant to the Earth's atmosphere.

Therefore, we included $N_2 - H_2O$ CIA from the classical molecular dynamics calculations of Hartmann et al., 2018b. This approach is very similar to that used previously for the overtone band of $N_2 - N_2$ and $N_2 - O_2$, as discussed in Section 3.3. Molecular dynamics simulations were performed with an anisotropic $N_2 - H_2O$ intermolecular potential and an induced dipole limited to its long range components based on the electric multipoles and polarizabilities. These classical simulations, free of any parameter adjusted to measurements, were corrected for the quantum nature of the Q transitions of H_2O, and lead to very satisfactory agreement with measurements as shown in Fig. 11. The model was then used for calculations at the temperatures of 270, 290, and 310 K more adapted to calculations dedicated to spectra of the Earth atmosphere (Hartmann, 2018).

3.16. Helium-containing collision pairs

It has been proposed that Helium-rich exoplanetary atmospheres may be relatively common (Hu et al., 2015). Hence, we included data of roto-translational spectra for some potentially-relevant helium-containing collision systems, namely $CH_4 - He$, $N_2 - He$, and $CO_2 - He$. The newly included spectra are shown in Fig. 12.

3.16.1. $CH_4 - He$

We here included the model line shapes by Taylor et al. (1988) for the roto-translational band of $CH_4 - He$ for frequencies up to 500 cm^{-1} and temperatures between 40 and 350 K. These model line shapes closely reproduce the calculations of Taylor et al. (1988), which were fit to experimental data from Bar-Ziv and Weiss (1972) and Afanas'ev et al. (1980). Thus, these are semiempirical rather than *ab initio* calculations. Therefore, they are best considered to yield smooth absorption spectra that closely reproduce the experimental data, with a smooth temperature dependence. It was shown more recently that pure *ab initio* calculations are not in agreement with these experimental results, presumably due to frame distortions of the tetrahedral CH_4 molecule, which are not included (Buser and Frommhold, 2005). These were also not included in the older calculations included here (Taylor et al., 1988), but these effectively corrected for this effect by fitting the dipole function to the experimental absorption spectrum.

3.16.2. $N_2 - He$ and $CO_2 - He$

For $N_2 - He$ and $CO_2 - He$, we also provide roto-translational bands for frequencies up to 1000 cm^{-1} at $T = 300$ K. In this case, we used only the "isotropic overlap term" modeled by a K_0 line shape, the definitions of which are found in Taylor et al. (1988). The experimental data were taken from Bar-Ziv and Weiss (1972), by digitizing Fig. 2 of that paper. The model line shapes were fit to these experimental data.

3.17. $H_2 - H_2$ low-temperature roto-translational band

Interaction-induced absorption of pairs of hydrogen molecules are of great importance for the opacity of the atmospheres of the four giant planets of our solar system. At temperatures typical for these atmospheres a small, but significant, fraction of the hydrogen molecules will be attached to each other in $(H_2)_2$ dimers. The dimers add sharp structures to the otherwise quasi-continuous collision-induced spectrum. Decades ago, these features were identified in the spectra of Jupiter and Saturn, recorded in the Voyager mission (Frommhold et al., 1984; McKellar, 1984), and they have been studied both in the laboratory (McKellar, 1988) and theoretically (Meyer et al., 1989).

Here we report on recently computed absorption data for pure hydrogen, which includes dimer features. It is an extension of the existing data set (Orton et al., 2007), which has no dimer contributions. Details of the computations, and applications of the data in modeling of planetary spectra, are available in Fletcher et al. (2018). The computations are based on the potential energy surface from Schäfer and Köhler (1989) and the dipole surface from Meyer et al. (1989). The dynamics are treated quantum mechanically and the full anisotropic potential is accounted for in the case of bound-to-bound transitions. In all transitions where continuum states are involved, the isotropic potential approximation is applied. This choice is based on prior computational investigations (Gustafsson et al., 2003; Karman et al., 2015b). In Fig. 13 the computed data are compared with laboratory measurements. Satisfactory agreement is observed in this and further comparisons (Fletcher et al., 2018) with experiments.

The HITRAN database now includes these spectra for frequencies up to 2400 cm^{-1}, at 10 temperatures, from 40 to 400 K. Data are available for both equilibrium H_2 and normal H_2, which has a 3:1 ortho:para ratio, as well as for 10 other out-of-equilibrium ortho:para ratios that can be used to model diffusion between atmospheric layers of different temperatures (see also Section 6) Modeling of giant planet spectra with the new absorption data as input reproduces the dimer features observed for all four giant planets (Fletcher et al., 2018). The need of out-of-equilibrium hydrogen in the modeling is generally reduced.

4. Atmospheric validations

The $O_2 - Air$ CIA has been validated using a portable ground-based FTS, which measures direct solar radiation from 5600 to 12,000 cm^{-1} at a spectral resolution of 0.5 cm^{-1} (Gisi et al., 2012; Chen et al., 2016). The O_2 CIA is easily discernible in the high air-mass spectra at the $a^1\Delta_g \leftarrow X^3\Sigma_g^-(0,0)$ band at 1.27 μm and the $a^1\Delta_g \leftarrow X^3\Sigma_g^-(1,0)$ band at 1.06 μm (Fig. 14a–b, d–e). The O_2 lines at the $a^1\Delta_g \leftarrow X^3\Sigma_g^-(0,0)$ band have been widely used by the ground-based FTS to retrieve air mass (Yang et al., 2002 Wunch et al., 2011a), but the O_2 CIA was usually only treated empirically (Kiel et al., 2016). Here we include the updated HITRAN $O_2 - Air$ CIA in the line-by-line forward model. The H_2O, CO_2, and O_2 line parameters are from HITRAN 2016 (Gordon et al., 2017) assuming a Voigt profile. Pressure, temperature, and CO_2/H_2O vertical profiles were adopted from the GGG2014 Software Suite (Wunch et al., 2011b). In addition, a scalar continuum level and a linear tilt are included in the fitting. The residual between the observed FTS spectra and the forward model is minimized using Levenberg–Marquardt nonlinear least square fitting.

Fig. 14 shows fits to an FTS spectrum collected at Cambridge, MA (42.377162 N, −71.113461 W) at 20:07:43 EDT on 24 June 2016. The $a^1\Delta_g \leftarrow X^3\Sigma_g^-(0,0)$ band is shown by Fig. 14a–c, where the empirical pseudo line list from GGG2014, which was derived from multiple laboratory and atmospheric spectra, empirically-adjusted theoretical CIA spectra from Karman et al. (2018), and the experimental CIA spectra from Maté et al. (1999) were tested in the fitting. The spectrum from Karman et al. (2018) captures the general shape and shows less kurtosis than the experimental spectra and the FTS atmospheric observation. The fitting residuals shown in Fig. 14c also reflect minor deviations of theoretical CIA from observation near 7950 cm^{-1}. Similarly, the fitting results for the $a^1\Delta_g \leftarrow X^3\Sigma_g^-(1,0)$ band are shown in Fig. 14d–f. The experimental CIA spectrum is from Karman et al. (2018) and shows the best agreement with FTS atmospheric observation.

5. Wish-list

While many interacting CIA pairs have yet to be studied experimentally and/or theoretically, some are of more importance to atmospheric studies than others. As we have discussed, $CO_2 - CO_2$, $CO_2 - H_2$, and $CO_2 - CH_4$ all deserve more detailed studyin the critical 0–1000 cm^{-1} wavelength range in the future. For early Earth and exoplanet applications, the interaction of H_2O with other species also deserves further study. In some exoplanet atmospheres, noble gases (He, Ne, and Ar) may be significantly more abundant than in the atmospheres of Earth, Venus, and Mars, and so their interaction with absorbers like CO_2 and H_2O also deserves detailed analysis.

In the near future, it will probably be most feasible to maintain a focus on the relatively low wavenumber regime and an Earth-like temperature regime (~150–350 K). However, CIA processes are also likely to be important for hotter planets, including those with a surface magma ocean, as may have been the case for the early Earth and Venus (*e.g.*, Zahnle et al., 2007). For this reason, CIA calculations or experiments up to higher temperatures and wavenumbers are also desired.

5.1. Astrophysical applications

The importance of collision-induced absorption by $H_2 - H_2$ and $H_2 - He$ in astrophysical applications, including acting as a coolant in star formation, and affecting the spectra of stars, is well recognized and summarized in the review paper, Abel and Frommhold, 2013. Other atomic species, as well as strongly bound molecules, may also have significant abundances in stellar atmospheres.

Table 2
Typical M dwarf number densities, in molecule cm^{-3}, of abundant atoms and molecules without significant monomer absorption, as a function of optical depth and temperature. Numbers in parentheses denote powers of ten.

τ_{Ross}	T/K	$n(H_2)$	$n(N_2)$	$n(O_2)$	n(He)	n(Ne)	n(Ar)
1.0(−05)	2011	6.91(13)	9.33(09)	3.75(05)	1.62(13)	2.05(10)	6.04(08)
1.0(−04)	2179	5.29(14)	7.13(10)	3.44(06)	1.24(14)	1.56(11)	4.61(09)
1.0(−03)	2430	2.72(15)	4.89(11)	5.40(07)	8.50(14)	1.07(12)	3.16(10)
1.0(−02)	2790	1.81(16)	3.00(12)	1.03(09)	5.22(15)	6.59(12)	1.94(11)
1.0(−01)	3248	7.41(16)	1.54(13)	1.08(10)	2.72(16)	3.43(13)	1.01(12)
1.0(−00)	3827	2.01(17)	5.77(13)	4.37(10)	1.10(17)	1.38(14)	4.08(12)
1.0(01)	4522	3.11(17)	1.09(14)	6.91(10)	3.07(17)	3.87(14)	1.14(13)
1.0(02)	5377	2.89(17)	4.94(13)	7.28(10)	6.37(17)	8.03(14)	2.37(13)

Table 2 shows number densities of various species, as a function of Rosseland optical depth in the atmosphere, that result from a schematic model photosphere for a typical M dwarf with effective temperature 3500 K, log surface gravity 5.0, and solar abundances (Kurucz and Robert, 2017). Included in the table are number densities for atoms and molecules that are relatively abundant but that do not have significant allowed transitions in the near UV, visible, and IR at these temperatures. These species collide with each other which gives rise to collision-induced absorption through the IR to the UV. Except for $H_2 - H_2$ and $H_2 - He$ (Abel et al., 2011 Abel et al., 2012b), these species have not been investigated at stellar temperatures. They may be strong or irrelevant. From the table it is clear that there are significant densities for N_2 and for Ne in addition to H_2 and He. A wish list of collision-induced absorption data includes the pairs $N_2 - H_2$, $N_2 - He$, $N_2 - Ne$, $N_2 - N_2$, and $H_2 - Ne$ for M dwarf stars, for temperature up to several thousand kelvin and for extended wavenumber ranges. Lower temperatures are also relevant to brown dwarfs.

6. Remarks on spin statistics

The previous release of HITRAN CIA has generated questions regarding the recommended data for different spin-statistics, effectively for H_2. At low temperature, the ortho-para ratio of H_2 at thermal equilibrium ($eq - H_2$) differs from 3:1, with the para contribution being enhanced. If H_2 is cooled down in the absence of a magnetic catalyst, the nuclear spin ratio will not change on experimentally relevant time scales, and one can record spectra of "normal" H_2 ($n - H_2$) which has a 3:1 ortho:para ratio even at lower temperature.

For $H_2 - He$ and $H_2 - H_2$, the recommended data in the Main folder are available for temperatures above 200 K, where there is essentially no distinction between normal and equilibrium H_2. For $H_2 - He$, the Alternate folder contains data down to $T = 40$ K for both $n - H_2$ and $eq - H_2$.

For $H_2 - H_2$, data down to $T = 40$ K is provided for $eq - H_2$, $n - H_2$, and a range of intermediate non-thermal ortho:para ratios, that can be used to model sub-equilibrium H_2 resulting from diffusion between atmospheric layers of different temperatures (Fletcher et al., 2018). Questions have been raised concerning the temperature range between 200 and 400 K, where the data sets overlap but do not agree exactly. In this range, the data in the Main folder is recommended. The data in the alternative directory is therefore necessary only for low temperatures, where the differences between $n - H_2$ and $eq - H_2$ are significant. As shown for $H_2 - He$ in Fig. 15 (Borysow et al., 1988), the effect of the spin statistics is pronounced at the lowest temperature, $T = 40$ K, but has disappeared well before $T = 200$ K, where both data sets overlap. Applications to hot Jupiters and brown dwarfs should not be concerned with the effect of spin statistics, and should use the recommended data in the Main folder.

7. Conclusions

Collision-induced absorption plays an appreciable role in the total absorption of radiation in atmospheres of terrestrial and extra-solar planets, cool white dwarfs, brown dwarfs, cool main sequence stars, so-called first stars, *etc.* It is not surprising that our original effort (Richard et al., 2012) of adding CIA parameters for different collisional partners to the HITRAN database was warmly welcomed by atmospheric scientists and astrophysicists. Nevertheless, there is a growing demand to improve and especially extend existing CIA data in HITRAN. This is in part due to anticipation of future observations of exoplanetary atmospheres that will have extremely diverse atmospheres in terms of constituents, temperature, and pressure. Remaining deficiencies described in the Richard et al. (2012) paper have inspired many new laboratory measurements and theoretical calculations. Here we made use of most recent available laboratory and theoretical results and carried out a substantial update to the CIA section in HITRAN. The update features improvements to the existing data, extension of spectral and temperature ranges as well as addition of new collisional pairs. Fig. 1 summarizes the current state of the CIA section in HITRAN including this update, and extensive details about the origin and choices of data are given throughout the paper. Remaining white cells in Fig. 1 as well as Section *5* indicate that this work by no means is complete and more measurements and calculations as well as their validations are needed. Once sufficient amounts of new information will become available, the next update of the CIA section will be issued.

It is worth noting that sometimes it is non-trivial to track down the actual data in the published articles. In fact we had a paper about this (Gordon et al., 2016). We strongly encourage scientists to report their data in the supplementary materials of the journals or (a much less preferable option) on some well-maintained internet resources before the data are lost permanently.

Instructions for accessing the CIA section of the HITRAN database can be found on the HITRAN website (www.hitran.org/cia). We also provide the data as supplementary material to this paper. Note that, unlike the website, the supplementary materials contain only new (with respect to Richard et al. (2012) effort) or updated data. Unlike the *line-by-line* and *cross-sections* parts of the HITRAN database which are cast into the SQL structure described in Hill et al. (2016), the CIA files are still provided in static ASCII format accompanied with a reference Table. In the near future, CIA parameters will also be cast into SQL structure. Access through the HITRAN Application Programming Interface (HAPI) (Kochanov et al., 2016) will also be enabled. Thus, calculations of absorption coefficients, cross-sections, *etc.* using HAPI will be implemented.

New data from a number of recent papers devoted to the CIA of different collisions (Mondelain et al., 2018 Banerjee et al., n.d. Turbet et al., 2019), will be evaluated for the next update of the CIA section. If their validation is successful, these data will appear in the next edition of the HITRAN database in 2020. Special consideration will be given to the O_2-N_2 and effectively O_2-Air in the region of the O_2 fundamental (covering the region of 1200–1900 cm^{-1}). As can be seen from Table 1, at the moment, HITRAN contains only O_2-O_2 data in that region from (Baranov et al., 2004). The most recent papers that report comprehensive studies of O_2-N_2 CIA in that region are Thibault et al. (1997)

and Maté et al. (2000). Unfortunately, it was established that the data from Maté et al. (2000) (which claims much smaller uncertainties than Thibault et al. (1997)) are permanently lost, leaving digitizing the plots that were given for some of the cross-sections as the only option. However, in the process of the revision of our paper we were able to find the data behind (Thibault et al., 1997). The existing data will be evaluated and included in the next edition of the database.

While the experimental data presented in this paper effectively contain isotopologues in their natural terrestrial abundances, the theoretical data do not have isotopic contributions included. This is something to keep in mind. However the importance of these contributions for interpreting planetary atmospheres may be quite small, although it is worth looking into HD–H_2 CIA. It is also an interesting system from a theoretical point of view as in HD, which has a small dipole moment, interference can be observed between the permanent and the interaction-induced dipoles (Tabisz, 2010).

Due to the numerous requests from the user community to include water continuum into HITRAN, some explanations are in order. Indeed the physical nature of the water continuum has much in common with the CIA. Interaction among water vapor molecules and molecules contributes to the overall "water" continuum, which has to be interpreted in terms of CIA. However, modification of the CIA theory to describe the water continuum is overly complicated since contributions from permanent and induced dipoles are heavily entangled in the case of interacting molecules with permanent dipole moments. So far, no theory could accurately model the continuum, and the different contributions are difficult to separate in experimental spectra. Nevertheless, some empirical models of the water continuum exist and we refer readers to the MT_CKD model, which is arguably the best model that currently exists (Mlawer et al., 2012).

Acknowledgements

The development of the CIA section of the HITRAN database is supported through the NASA Aura and NASA PDART grants NNX17AI78G and NNX16AG51G, respectively. T.K. is supported by NWO Rubicon grant 019.172EN.007 and an NSF grant to ITAMP. Part of the research described in this article was performed at the Jet Propulsion Laboratory, California Institute of Technology and at Space Science Laboratory, University of Berkeley, California, under contracts and cooperative agreements with the National Aeronautics and Space Administration. R.V. thanks Henning Finkenzeller for helpful discussions and testing of their O_2-O_2 cross-section data files. M.G. acknowledges support from the Knut and Alice Wallenberg Foundation. A.V. appreciates invaluable contribution from his collaborators and partial support from RFBR Grants 18-05-0019 and 18-32-20156, and CNRS-RFBR project 18-55-16006. In the process of preparation of this manuscript one of our dear coauthors, Dr. Yury Baranov, passed away. His contribution to this work and to the general understanding of collision-induced absorption and water continuum are indispensable. It is to him we wish to dedicate this paper.

Appendix A. Supplementary data

Supplementary data to this article can be found online at https://doi.org/10.1016/j.icarus.2019.02.034.

References

Abel, M., Frommhold, L., 2013. Collision-induced spectra and current astronomical research gas of H_2. Can. J. Phys. 91, 0532. https://doi.org/10.1139/cjp-2012-0532.

Abel, M., Frommhold, L., Li, X., Hunt, K.L.C., 2011. Collision-induced absorption by H_2 pairs: from hundreds to thousands of Kelvin. J. Phys. Chem. A 115 (25), 6805–6812. https://doi.org/10.1021/jp109441f.

Abel, M., Frommhold, L., Li, X., Hunt, K.L.C., 2012a. Infrared absorption by collisional H_2–He complexes at temperatures up to 9000 K and frequencies from 0 to 20000 cm^{-1}. J. Chem. Phys. 136 (4), 044319. https://doi.org/10.1063/1.3676405.

Abel, M., Frommhold, L., Li, X., Hunt, K.L.C., 2012b. Infrared absorption by collisional H_2–He complexes at temperatures up to 9000 K and frequencies from 0 to 20000 cm^{-1}. J. Chem. Phys. 136 (4), 044319. https://doi.org/10.1063/1.3676405.

Afanas'ev, A., Bulanin, M., Tonkov, M., 1980. Anisotropy of collisions in the CF_4 + He system. Sov. Tech. Phys. Lett. 6, 1444 (in Russian).

A. Banerjee, J. Mandon, F. Harren, D. H. Parker, Collision-induced absorption between O_2–CO_2 for the $a^1\Delta_g$ ($v = 1$)← $X^3\Sigma_g^-$ ($v = 0$) transition of molecular oxygen at 1060 nm, Phys. Chem. Chem. Phys. doi:https://doi.org/10.1039/C8CP06778C. http://xlink.rsc.org/?DOI=C8CP06778C

Baranov, Y., 2011. The continuum absorption in H_2O+N_2 mixtures in the 2000–3250 cm^{-1} spectral region at temperatures from 326 to 363K. J. Quant. Spectrosc. Radiat. Transf. 112 (14), 2281–2286. https://doi.org/10.1016/j.jqsrt.2011.06.005.

Baranov, Y., Vigasin, A., 1999. Collision-induced absorption by CO_2 in the region of ν_1, $2\nu_2$. J. Mol. Spectrosc. 193 (2), 319–325. https://doi.org/10.1006/jmsp.1998.7743.

Baranov, Y., Fraser, G.T., Lafferty, W.J., Vigasin, A., 2003a. Collision-induced absorption in the CO_2 fermi triad for temperatures from 211 K to 296 K. In: Camy-Peyret, C., Vigasin, A. (Eds.), Weakly Interacting Molecular Pairs: Unconventional Absorbers of Radiation in the Atmosphere. Springer, pp. 149–158.

Baranov, Y., Lafferty, W., Fraser, G., Vigasin, A., 2003b. On the origin of the band structure observed in the collision-induced absorption bands of CO_2. J. Mol. Spectrosc. 218 (2), 260–261. https://doi.org/10.1016/S0022-2852(02)00093-0.

Baranov, Y., Lafferty, W., Fraser, G., 2005. Investigation of collision-induced absorption in the vibrational fundamental bands of O_2 and N_2 at elevated temperatures. J. Mol. Spectrosc. 233 (1), 160–163. https://doi.org/10.1016/j.jms.2005.06.008.

Baranov, Y.I., 2018. Collision-induced absorption in the region of the $\nu_2+\nu_3$ band of carbon dioxide. J. Mol. Spectrosc. 345, 11–16. https://doi.org/10.1016/j.jms.2017.11.005.

Baranov, Y.I., Lafferty, W., Fraser, G., 2004. Infrared spectrum of the continuum and dimer absorption in the vicinity of the O_2 vibrational fundamental in O_2/CO_2 mixtures. J. Mol. Spectrosc. 228 (2), 432–440. Special Issue Dedicated to Dr. Jon T. Hougen on the Occasion of His 68th Birthday. https://doi.org/10.1016/j.jms.2004.04.010.

Baranov, Y.I., Buryak, I.A., Lokshtanov, S.E., Lukyanchenko, V.A., Vigasin, A.A., 2012. H_20–N_2 collision-induced absorption band intensity in the region of the N_2 fundamental: ab initio investigation of its temperature dependence and comparison with laboratory data. Phil. Trans. R. Soc. A 370 (1968), 2691–2709. https://doi.org/10.1098/rsta.2011.0189.

Bar-Ziv, E., Weiss, S., 1972. Translational spectra due to collision-induced overlap moments in mixtures of He with CO_2, N_2, CH_2, and C_2H_6. J. Chem. Phys. 57, 34. https://doi.org/10.1063/1.1677970.

Birnbaum, G., 1978. Far-infrared absorption in H_2 and H_2-He mixtures. J. Quant. Spectrosc. Radiat. Transf. 19, 51–62. https://doi.org/10.1016/0022-4073(78)90039-0.

Borysow, A. Fortran programs and data for modeling CIA opacities of various molecular complexes for application to planetary and stellar atmospheres. http://www.astro.ku.dk/aborysow/programs/index.html.

Borysow, A., Frommhold, L., 1986a. Theoretical collision-induced rototranslational absorption spectra for the outer planets-H_2–CH_4 pairs. Astrophys. J. 304, 849–865.

Borysow, A., Frommhold, L., 1986b. Theoretical collision-induced rototranslational absorption spectra for modeling Titan's atmosphere-H_2–N_2 pairs. Astrophys. J. 303, 495–510.

Borysow, A., Frommhold, L., 1986c. Collision-induced rototranslational absorption spectra of N_2-N_2 pairs for temperatures from 50 to 300 K. Astrophys. J. 311, 1043–1057. https://doi.org/10.1086/164841.

Borysow, A., Frommhold, L., 1987. Collision-induced rototranslational absorption spectra of CH_4–CH_4 pairs at temperatures from 50 to 300 K. Astrophys. J. 318, 940–943.

Borysow, A., Tang, C., 1993. Far infrared CIA spectra of N_2–CH_4 pairs for modeling of Titan's atmosphere. Icarus 105 (1), 175–183.

Borysow, A., Frommhold, L., Birnbaum, G., 1988. Collision-induced rototranslational absorption spectra of H_2–He pairs at temperatures from 40 to 3000 K. Astrophys. J. 326, 509.

Bouanich, J., 1992. Site-site Lennard-Jones potential parameters for N_2, O_2, H_2, CO and CO_2. J. Quant. Spectrosc. Radiat. Transf. 47, 243. https://doi.org/10.1016/0022-4073(92)90142-Q.

Buser, M., Frommhold, L., 2005. Infrared absorption by collisional CH_4+X pairs, with X = He, H_2, or N_2. J. Chem. Phys. 122, 024301. https://doi.org/10.1063/1.1829055.

Chen, J., Viatte, C., Hedelius, J.K., Jones, T., Franklin, J.E., Parker, H., Gottlieb, E.W., Wennberg, P.O., Dubey, M.K., Wofsy, S.C., 2016. Differential column measurements using compact solar-tracking spectrometers. Atmos. Chem. Phys. 16 (13), 8479–8498. https://doi.org/10.5194/acp-16-8479-2016. https://www.atmos-chem-phys.net/16/8479/2016/.

Chimot, J., Veefkind, J.P., Vlemmix, T., de Haan, J.F., Amiridis, V., Proestakis, E., Marinou, E., Levelt, P.F., 2017. An exploratory study on the aerosol height retrieval from OMI measurements of the 477 nm O_2–O_2 spectral band using a neural network approach. Atmos. Meas. Tech. 10, 783–809. https://doi.org/10.5194/amt-10-783-2017. https://www.atmos-meas-tech.net/10/783/2017/.

Dagg, I.R., Anderson, A., Yan, S., Smith, W., Read, L.A.A., 1985. Collision-induced absorption in nitrogen at low temperatures. Can. J. Phys. 63, 625.

Drouin, B.J., Benner, D.C., Brown, L.R., Cich, M.J., Crawford, T.J., Devi, V.M., Guillaume, A., Hodges, J.T., Mlawer, E.J., Robichaud, D.J., Oyafuso, F., Payne, V.H., Sung, K., Wishnow, E.H., Yu, S., 2017. Multispectrum analysis of the oxygen A-band. J. Quant. Spectrosc. Radiat. Transf. 186, 118. https://doi.org/10.1016/j.jqsrt.2016.03.037.

Dudhia, A., 2017. The reference forward model (RFM). J. Quant. Spectrosc. Radiat. Transf. 186, 243–253. https://doi.org/10.1016/j.jqsrt.2016.06.018. http://linkinghub.elsevier.com/retrieve/pii/S0022407316301029.

Fletcher, L.N., Gustafsson, M., Orton, G.S., 2018. Hydrogen dimers in giant-planet

infrared spectra. Astrophys. J. Suppl. Ser. 235 (1), 24.
Fortney, J.J., Robinson, T.D., Domagal-Goldman, S., Skålid Amundsen, D., Brogi, M., Claire, M., Crisp, D., Hebrard, E., Imanaka, H., de Kok, R., Marley, M.S., Teal, D., Barman, T., Bernath, P., Burrows, A., Charbonneau, D., Freedman, R.S., Gelino, D., Helling, C., Heng, K., Jensen, A.G., Kane, S., Kempton, E.M.-R., Kopparapu, R.K., Lewis, N.K., Lopez-Morales, M., Lyons, J., Lyra, W., Meadows, V., Moses, J., Pierrehumbert, R., Venot, O., Wang, S.X., Wright, J.T., 2016. The Need for Laboratory Work to Aid in the Understanding of Exoplanetary Atmospheres. arXiv e-printsarXiv:1602.06305.
Frommhold, L., 2006. Collision-Induced Absorption in Gases. Cambridge Univ. Press, Cambridge.
Frommhold, L., Samuelson, R., Birnbaum, G., 1984. Hydrogen dimer structures in the far-infrared spectra of Jupiter and Saturn. Astrophys. J. Lett. 283, L79–L82. https://doi.org/10.1086/184338.
Gandhi, S., Madhusudhan, N., 2018. Retrieval of exoplanet emission spectra with HyDRA. Mon. Not. R. Astron. Soc. 474 (1), 271–288. https://doi.org/10.1093/mnras/stx2748. http://academic.oup.com/mnras/article/474/1/271/4563628.
Gisi, M., Hase, F., Dohe, S., Blumenstock, T., Simon, A., Keens, A., 2012. Xco$_2$-measurements with a tabletop FTS using solar absorption spectroscopy. Atmos. Meas. Tech. 5 (11), 2969–2980. https://doi.org/10.5194/amt-5-2969-2012. https://www.atmos-meas-tech.net/5/2969/2012/.
Gordon, I.E., Kassi, S., Campargue, A., Toon, G.C., 2010. First identification of the $a^1\Delta_g - X^3\Sigma_g^-$ electric quadrupole transitions of oxygen in solar and laboratory spectra. J. Quant. Spectrosc. Radiat. Transf. 111 (9), 1174–1183. https://doi.org/10.1016/j.jqsrt.2010.01.008. 000191. http://linkinghub.elsevier.com/retrieve/pii/S0022407310.
Gordon, I.E., Potterbusch, M.R., Bouquin, D., Erdmann, C.C., Wilzewski, J.S., Rothman, L.S., 2016. Are your spectroscopic data being used? J. Mol. Spectrosc. 327, 232–238. https://doi.org/10.1016/j.jms.2016.03.011. http://linkinghub.elsevier.com/retrieve/pii/S0022285216300388.
Gordon, I.E., Rothman, L.S., Hill, C., Kochanov, R.V,, Tan, Y., Bernath, P.F., Birk, M., Boudon, V., Campargue, A., Chance, K.V., Drouin, B.J., Flaud, J.-M., Gamache, R.R., Hodges, J., Jacquemart, D., Perevalov, V.I., Perrin, A., Shine, K., Smith, M.-A., Tennyson, J., Toon, G., Tran, H., Tyuterev, V., Barbe, A., Császár, A., Devi, V., Furtenbacher, T., Harrison, J., Hartmann, J.-M., Jolly, A., Johnson, T., Karman, T., Kleiner, I., Kyuberis, A., Loos, J., Lyulin, O., Massie, S., Mikhailenko, S., Moazzen-Ahmadi, N., Müller, H., Naumenko, O., Nikitin, A., Polyansky, O., Rey, M., Rotger, M., Sharpe, S., Sung, K., Starikova, E., Tashkun, S., Auwera, J.V., Wagner, G., Wilzewski, J., Wcisło, P., Yu, S., Zak, E., 2017. The HITRAN2016 molecular spectroscopic database. J. Quant. Spectrosc. Radiat. Transf. 203, 3. https://doi.org/10.1016/j.jqsrt.2017.06.038.
Greenblatt, G.D., Orlando, J.J., Burkhoder, J.B., Ravishankara, A.R., 1990. Absorption measurements of oxygen between 330 and 1140 nm. J. Geophys. Res. 95, 18577. https://doi.org/10.1029/JD095iD11p18577.
Gruszka, M., Borysow, A., 1997. Roto-translational collision-induced absorption of CO_2 for the atmosphere of Venus at frequencies from 0 to 250 cm^{-1}, at temperatures from 200 to 800 K. Icarus 129, 172. https://doi.org/10.1006/icar.1997.5773.
Gustafsson, M., Frommhold, L., 2001. Infrared absorption spectra of collisionally interacting He and H atoms. Astrophys. J. 546 (2), 1168.
Gustafsson, M., Frommhold, L., 2003. The H_2–H infrared absorption bands at temperatures from 1000 K to 2500 K. Astron. Astrophys. 400 (3), 1161–1162. https://doi.org/10.1051/0004-6361:20030100.
Gustafsson, M., Frommhold, L., Bailly, D., Bouanich, J.-P., Brodbeck, C., 2003. Collision-induced absorption in the rototranslational band of dense hydrogen gas. J. Chem. Phys. 119, 12264–12270. https://doi.org/10.1063/1.1625635.
Hartmann, J.-M., 2018. Indirect Influence of Humidity on Atmospheric Spectra Near 4 µm. in preparation. .
Hartmann, J.-M., Boulet, C., Jacquemart, D., 2011. Molecular dynamics simulations for CO_2 spectra. ii. The far infrared collision-induced absorption band. J. Chem. Phys. 134 (9), 094316. https://doi.org/10.1063/1.3557681.
Hartmann, J.-M., Boulet, C., Toon, G.C., 2017. Collision-induced absorption by N_2 near 2.16 µm: calculations, model, and consequences for atmospheric remote sensing. J. Geophys. Res. Atmos. 122, 2419. https://doi.org/10.1002/2016JD025677.
Hartmann, J.-M., Tran, H., Armante, R., Boulet, C., Campargue, A., Forget, F., Gianfrani, L., Gordon, I., Guerlet, S., Gustafsson, M., Hodges, J.T., Kassi, S., Lisak, D., Thibault, F., Toon, G.C., 2018a. Recent advances in collisional effects on spectra of molecular gases and their practical consequences. J. Quant. Spectrosc. Radiat. Transf. 213, 178–227. https://doi.org/10.1016/j.jqsrt.2018.03.016.
Hartmann, J.-M., Boulet, C., Tran, D.D., Tran, H., Baranov, Y., 2018b. Effect of humidity on the absorption continua of CO_2 and N_2 near 4 µm: calculations, comparisons with measurements, and consequences for atmospheric spectra. J. Chem. Phys. 148 (5), 054304. https://doi.org/10.1063/1.5019994.
Hermans, C. Measurement of Absorption Cross Sections and Spectroscopic Molecular Parameters. http://spectrolab.aeronomie.be/o2.htm.
C. Hill, I. E. Gordon, R. V. Kochanov, L. Barrett, J. S. Wilzewski, L. S. Rothman, HITRANonline: an online interface and the flexible representation of spectroscopic data in the HITRAN database, J. Quant. Spectrosc. Radiat. Transf. 177 (2016) 4–14. doi:https://doi.org/10.1016/j.jqsrt.2015.12.012. http://www.sciencedirect.com/science/article/pii/S00224 07315302375.
Hollis, M., Tessenyi, M., Tinetti, G., 2013. TAU: a 1D radiative transfer code for transmission spectroscopy of extrasolar planet atmospheres. Comput. Phys. Commun. 184 (10), 2351–2361. https://doi.org/10.1016/j.cpc.2013.05.011. http://linkinghub.elsevier.com/retrieve/pii/S0010465513001719.
Hu, R., Seager, S., Yung, Y.L., 2015. Helium atmospheres on warm Neptune- and sub-Neptune-sized exoplanets and applications to GJ436b. Astrophys. J. 807 (1), 8. https://doi.org/10.1088/0004-637X/807/1/8.
Huisken, F., Ramonat, L., Santos, J., Smirnov, V., Stelmakh, O., Vigasin, A., 1997. High-resolution CARS spectroscopy of small carbon dioxide clusters: investigation of the CO_2 dimer in the $\nu_1/2\nu_2$ Fermi dyad. J. Mol. Struct. 410-411 (Supplement C), 47–50. https://doi.org/10.1016/S0022-2860(96)09664-0.
Joalland, B., Goubet, M., Georges, R., Manceron, L., Vigasin, A., 2016. Far-Infrared Collision-Induced Absorption in CO_2 at T = 200 K, ASA - HITRAN Congress, Aug 2016, Reims, France.
Karman, T., Miliordos, E., Hunt, K.L.C., Groenenboom, G.C., van der Avoird, A., 2015a. Quantum mechanical calculation of the collision-induced absorption spectra of N_2–N_2 with anisotropic interactions. J. Chem. Phys. 142, 084306. https://doi.org/10.1063/1.4907917.
Karman, T., van der Avoird, A., Groenenboom, G.C., 2015b. Collision-induced absorption with exchange effects and anisotropic interactions: theory and application to H_2–H_2. J. Chem. Phys. 142 (8). https://doi.org/10.1063/1.4907916.
Karman, T., Koenis, M.A.J., Banerjee, A., Parker, D.H., Gordon, I.E., van der Avoird, A., van der Zande, W.J., Groenenboom, G.C., 2018. O_2–O_2 and O_2 − N_2 collision-induced absorption mechanisms unravelled. Nat. Chem. 10, 549. https://doi.org/10.1038/s41557-018-0015-x. https://rdcu.be/K2fO.
Kataoka, F., Crisp, D., Taylor, T., O'Dell, C., Kuze, A., Shiomi, K., Suto, H., Bruegge, C., Schwandner, F., Rosenberg, R., Chapsky, L., Lee, R., 2017. The cross-calibration of spectral radiances and cross-validation of CO_2 estimates from GOSAT and OCO_2. Remote Sens. 9 (12), 1158. https://doi.org/10.3390/rs9111158. http://www.mdpi.com/2072-4292/9/11/1158.
Kiel, M., Wunch, D., Wennberg, P.O., Toon, G.C., Hase, F., Blumenstock, T., 2016. Improved retrieval of gas abundances from near-infrared solar FTIR spectra measured at the Karlsruhe TCCON station. Atmos. Meas. Tech. 9 (2), 669–682. https://doi.org/10.5194/amt-9-669-2016. https://www.atmos-meas-tech.net/9/669/2016/.
Kochanov, R.V., Gordon, I.E., Rothman, L.S., Wcisło, P., Hill, C., Wilzewski, J.S., 2016. HITRAN application programming Interface (HAPI): a comprehensive approach to working with spectroscopic data. J. Quant. Spectrosc. Radiat. Transf. 177, 15–30. https://doi.org/10.1016/j.jqsrt.2016.03.005. http://www.sciencedirect.com/science/article/pii/S0022407315302466.
Kurucz, R.L., Robert, L., 2017. Kurucz's research home page. http://kurucz.harvard.edu/stars/gl411/xnfpat3500g50kv.log.
Lafferty, W.J., Solodov, A.M., Weber, A., Olson, W.B., Hartmann, J.-M., 1996. Infrared collision-induced absorption by N_2 near 4.3 µm for atmospheric applications: measurements and empirical modeling. Appl. Opt. 35 (30), 5911. https://doi.org/10.1364/AO.35.005911. https://www.osapublishing.org/abstract.cfm?URI=ao-35-30-5911.
Lampel, J., Zielcke, J., Schmitt, S., Pöhler, D., Frieß, U., Platt, U., Wagner, T., 2018. Detection of O_4 absorption around 328 and 419 nm in measured atmospheric absorption spectra. Atmos. Chem. Phys. 18, 1671–1683. https://doi.org/10.5194/acp-18-1671-2018.
Lora, J.M., Lunine, J.I., Russell, J.L., 2015. GCM simulations of Titan's middle and lower atmosphere and comparison to observations. Icarus 250, 516–528. https://doi.org/10.1016/j.icarus.2014.12.030. http://linkinghub.elsevier.com/retrieve/pii/S0019103514007210.
Malik, M., Grosheintz, L., Mendonça, J.M., Grimm, S.L., Lavie, B., Kitzmann, D., Tsai, S.-M., Burrows, A., Kreidberg, L., Bedell, M., Bean, J.L., Stevenson, K.B., Heng, K., 2017. HELIOS: an open-source, GPU-accelerated radiative transfer code for self-consistent exoplanetary atmospheres. Astron. J. 153 (2), 56. https://doi.org/10.3847/1538-3881/153/2/56. http://stacks.iop.org/1538-3881/153/i=2/a=56?key=crossref.13be324335b57f6e5406224211f955f6.
Maté, B., Lugez, C., Fraser, G.T., Lafferty, W.J., 1999. Absolute intensities for the O_2 1.27 µm continuum absorption. J. Geophys. Res. Atmos. 104 (D23), 30585–30590. https://doi.org/10.1029/1999JD900824.
Maté, B., Lugez, C.L., Solodov, A.M., Fraser, G.T., Lafferty, W.J., 2000. Investigation of the collision-induced absorption by O_2 near 6.4 μm in pure O_2 and O_2/N_2 mixtures. J. Geophys. Res. Atmos. 105 (D17), 22225–22230. https://doi.org/10.1029/2000JD900295. http://doi.wiley.com/10.1029/2000JD900295.
McKellar, A., 1989. Low-temperature infrared absorption of gaseous N_2 and N_2 + H_2 in the 2.02.5 µm region: application to the atmospheres of titan and triton. Icarus 80 (2), 361–369. https://doi.org/10.1016/0019-1035(89)90146-2.
McKellar, A.R.W., 1984. Possible identification of sharp features in the Voyager far-infrared spectra of Jupiter and Saturn. Can. J. Phys. 62, 760–763. https://doi.org/10.1139/p84-104.
McKellar, A.R.W., 1988. Experimental verification of hydrogen dimers in the atmospheres of Jupiter and Saturn from Voyager IRIS far-infrared spectra. Astrophys. J. Lett. 326, L75–L77. https://doi.org/10.1086/185126.
Meadows, V.S., 2017. Reflections on O_2 as a biosignature in exoplanetary atmospheres. Astrobiology 17 (10), 1022–1052. https://doi.org/10.1089/ast.2016.1578. http://online.liebertpub.com/doi/10.1089/ast.2016.1578.
Menoux, V., Doucen, R.L., Boulet, C., Roblin, A., Bouchardy, A.M., 1993. Collision-induced absorption in the fundamental band of N_2: temperature dependence of the absorption for N_2-N_2 and N_2-O_2 pairs. Appl. Opt. 32 (3), 263–268. https://doi.org/10.1364/AO.32.000263.
Meyer, W., Frommhold, L., Birnbaum, G., 1989. Rototranslational absorption spectra of H_2–H_2 pairs in the far infrared. Phys. Rev. A 39, 2434–2448. https://doi.org/10.1103/PhysRevA.39.2434.
Mlawer, E.J., Payne, V.H., Moncet, J.-L., Delamere, J.S., Alvarado, M.J., Tobin, D.C., 2012. Development and recent evaluation of the MT_CKD model of continuum absorption. Philos. Trans. R. Soc. A Math. Phys. Eng. Sci. 370 (1968), 2520–2556. https://doi.org/10.1098/rsta.2011.0295. http://rsta.royalsocietypublishing.org/cgi/doi/10.1098/rsta.2011.0295.

Moazzen-Ahmadi, N., Norooz Oliaee, J., Ozier, I., Wishnow, E.H., Sung, K., Crawford, T.J., Brown, L.R., Devi, V.M., 2015. An intensity study of the torsional bands of ethane at 35 μm. J. Quant. Spectrosc. Radiat. Transf. 151, 123–132. https://doi.org/10.1016/j.jqsrt.2014.09.016.

Mondelain, D., Kassi, S., Campargue, A., 2018. Accurate laboratory measurement of the O_2 collision-induced absorption band near 1.27 μm. J. Geophys. Res. Atmos. https://doi.org/10.1029/2018JD029317. http://doi.wiley.com/10.1029/2018JD029317.

I. Ortega, L. K. Berg, R. A. Ferrare, J. W. Hair, C. A. Hostetler, R. Volkamer, Elevated aerosol layers modify the O_2–O_2 absorption measured by ground-BASED MAX-DOAS, J. Quant. Spectrosc. Radiat. Transf. 176 (2016) 34–49. doi:https://doi.org/10.1016/j.jqsrt.2016.02.021. http://linkinghub.elsevier.com/retrieve/pii/S0022407315 301746.

Orton, G.S., Gustafsson, M., Burgdorf, M., Meadows, V., 2007. Revised ab initio models for H_2-H_2 collision induced absorption at low temperatures. Icarus 189, 544–549.

Richard, C., Gordon, I., Rothman, L., Abel, M., Frommhold, L., Gustafsson, M., Hartmann, J.-M., Hermans, C., Lafferty, W., Orton, G., Smith, K., Tran, H., 2012. New section of the HITRAN database: collision-induced absorption (CIA). J. Quant. Spectrosc. Radiat. Transf. 113, 1276. https://doi.org/10.1016/j.jqsrt.2011.11.004.

Rothman, L.S., Gordon, I.E., Babikov, Y., Barbe, A., Chris Benner, D., Bernath, P., Birk, M., Bizzocchi, L., Boudon, V., Brown, L., Campargue, A., Chance, K., Cohen, E., Coudert, L., Devi, V., Drouin, B., Fayt, A., Flaud, J.-M., Gamache, R., Harrison, J., Hartmann, J.-M., Hill, C., Hodges, J., Jacquemart, D., Jolly, A., Lamouroux, J., Le Roy, R., Li, G., Long, D., Lyulin, O., Mackie, C., Massie, S., Mikhailenko, S., Müller, H., Naumenko, O., Nikitin, A., Orphal, J., Perevalov, V., Perrin, A., Polovtseva, E., Richard, C., Smith, M., Starikova, E., Sung, K., Tashkun, S., Tennyson, J., Toon, G., Tyuterev, V., Wagner, G., 2013. The HITRAN2012 molecular spectroscopic database. J. Quant. Spectrosc. Radiat. Transf. 130, 4–50. 002859. http://linkinghub.elsevier.com/retrieve/pii/S0022407313.

Samuelson, R.E., Nath, N.R., Borysow, A., 1997. Gaseous abundances and methane supersaturation in Titan's troposphere. Planet. Space Sci. 45 (8), 959–980.

Schäfer, J., Köhler, W.E., 1989. Low-temperature second virial coefficient of p-H_2 gas obtained from quantum mechanical pair correlation functions. Z. Physik D 13, 217–229.

Schreier, F., García, S. Gimeno, Hedelt, P., Hess, M., Mendrok, J., Vasquez, M., Xu, J., 2014. GARLIC a general purpose atmospheric radiative transfer line-by-line infrared-microwave code: implementation and evaluation. J. Quant. Spectrosc. Radiat. Transf. 137, 29–50. https://doi.org/10.1016/j.jqsrt.2013.11.018. http://linkinghub.elsevier.com/retrieve/pii/S0022407313004731.

Shapiro, M.M., Gush, H.P., 1966. The collision-induced fundamental and first overtone bands of oxygen and nitrogen. Can. J. Phys. 44 (5), 949–963. https://doi.org/10.1139/p66-079. http://www.nrcresearchpress.com/doi/10.1139/p66-079.

Sioris, C.E., Boone, C.D., Nassar, R., Sutton, K.J., Gordon, I.E., Walker, K.A., Bernath, P.F., 2014. Retrieval of carbon dioxide vertical profiles from solar occultation observations and associated error budgets for ACE-FTS and CASS-FTS. Atmos. Meas. Tech. 7 (7), 2243–2262. https://doi.org/10.5194/amt-7-2243-2014. http://www.atmos-meas-tech.net/7/2243/2014/.

Spiering, F.R., van der Zande, W.J., 2012. Collision induced absorption in the $a^1\Delta(\nu=2) \leftarrow X^3\Sigma_g^-(\nu=0)$ band of molecular oxygen. Phys. Chem. Chem. Phys. 14 (28), 9923–9928. https://doi.org/10.1039/c2cp40961e.

Spiering, F.R., Kiseleva, M.B., Filippov, N.N., van Kesteren, L., van der Zande, W.J., 2011. Collision-induced absorption in the O_2 B-band region near 670 nm. Phys. Chem. Chem. Phys. 13, 9616–9621. https://doi.org/10.1039/C1CP20403C.

Spinei, E., Cede, A., Herman, J., Mount, G.H., Eloranta, E., Morley, B., Baidar, S., Dix, B., Ortega, I., Koenig, T., Volkamer, R., 2014. Direct sun and airborne MAX-DOAS measurements of the collision induced oxygen complex, O_2–O_2 absorption with significant pressure and temperature differences. Atmos. Meas. Tech. Discuss. 7 (9), 10015–10057. https://doi.org/10.5194/amtd-7-10015-2014. http://www.atmos-meas-tech-discuss.net/7/10015/2014/.

Spinei, E., Cede, A., Herman, J., Mount, G.H., Eloranta, E., Morley, B., Baidar, S., Dix, B., Ortega, I., Koenig, T., Volkamer, R., 2015. Ground-based direct-sun DOAS and airborne MAX-DOAS measurements of the collision-induced oxygen complex, $O-2O_2$, absorption with significant pressure and temperature differences. Atmos. Meas. Tech. 8, 793–809. https://doi.org/10.5194/amt-8-793-2015.

Sung, K., Wishnow, E.H., Malathy Devi, V., Brown, L.R., Ozier, I., Benner, D.C., Crawford, T.J., Mantz, A.W., Smith, M.A.H., 2016. Progress in the measurement of temperature-dependent N_2-N_2 collision-induced absorption and H_2-broadening of cold and hot CH_4. In: American Astronomical Society, DPS Meeting #48, Pasadena.

Tabisz, G.C., 2010. Intra-collision effects in the collision-broadening of spectral line profiles. Int. Rev. Atom. Molec. Phys. 1 (June), 53–61.

Taylor, R.H., Borysow, A., Frommhold, L., 1988. Concerning the rototranslational absorption spectra of He–CH−4 pairs. J. Mol. Spectrosc. 129, 45. https://doi.org/10.1016/0022-2852(88)90257-3.

Thalman, R., Volkamer, R., 2013. Temperature dependent absorption cross-sections of O_2-O_2 collision pairs between 340 and 630 nm and at atmospherically relevant pressure. Phys. Chem. Chem. Phys. 15 (37), 15371. https://doi.org/10.1039/c3cp50968k.

Thibault, F., Menoux, V., Le Doucen, R., Rosenmann, L., Hartmann, J.-M., Boulet, C., 1997. Infrar ed collision-induced absorption by O_2 near 6.4 μm for atmospheric applications: measurements and empirical modeling. Appl. Opt. 36 (3), 563. https://doi.org/10.1364/AO.36.000563. https://www.osapublishing.org/ao/abstract.cfm?uri=ao-36-3-563.

Tran, H., Boulet, C., Hartmann, J.-M., 2006. Line mixing and collision-induced absorption by oxygen in the A-band: laboratory measurements, model, and tools for atmospheric spectra computations. J. Geophys. Res. 111, D15210. https://doi.org/10.1029/2005JD006869.

Turbet, M., Tran, H., Pirali, O., Forget, F., Boulet, C., Hartmann, J.-M., 2019. Far infrared measurements of absorptions by CH_4+CO_2 and H_2+CO_2 mixtures and implications for greenhouse warming on early Mars. Icarus 321, 189–199. https://doi.org/10.1016/J.ICARUS.2018.11.021. https://www.sciencedirect.com/science/article/pii/S0019103518303270.

Vangvichith, M., Tran, H., Hartmann, J.-M., 2009. Line-mixing and collision induced absorption for O_2 − CO_2 mixtures in the oxygen A-band region. J. Quant. Spectrosc. Radiat. Transf. 110 (18), 2212–2216. https://doi.org/10.1016/j.jqsrt.2009.06.002.

Wishnow, E.H., Gush, H.P., Ozier, I., 1996. Far-infrared spectrum of N_2 and N_2-noble gas mixtures near 80 k. J. Chem. Phys. 104, 3511–3516. https://doi.org/10.1063/1.471056.

Wishnow, E.H., Leung, A., Gush, H.P., 1999. Cryogenic multiple reflection absorption cell and Fourier transform spectrometer system for the far infrared. Rev. Sci. Instrum. 70, 23–31. https://doi.org/10.1063/1.1149537.

Wordsworth, R., Pierrehumbert, R., 2013. Hydrogen-nitrogen greenhouse warming in earth's early atmosphere. Science 339 (6115), 64. https://doi.org/10.1126/science.1225759.

Wordsworth, R., Forget, F., Eymet, V., 2010. Infrared collision-induced and far-line absorption in dense CO_2 atmospheres. Icarus 210 (2), 992–997. https://doi.org/10.1016/j.icarus.2010.06.010.

Wordsworth, R., Kalugina, Y., Lokshtanov, S., Vigasin, A., Ehlmann, B., Head, J., Sanders, C., Wang, H., 2017. Transient reducing greenhouse warming on early Mars. Geophys. Res. Lett. 44, 665. https://doi.org/10.1002/2016GL071766.

Wunch, D., Toon, G.C., Blavier, J.-F.L., Washenfelder, R.A., Notholt, J., Connor, B.J., Griffith, D.W., Sherlock, V., Wennberg, P.O., 2011a. The total carbon column observing network. Phil. Trans. R. Soc. A 369 (1943), 2087–2112.

Wunch, D., Toon, G.C., Sherlock, V., Deutscher, N.M., Liu, C., Feist, D.G, Wennberg, P.O., 2011b. The Total Carbon Column Observing network's GGG2014 Data Version. Carbon Dioxide Information Analysis Center, Oak Ridge National Laboratory, Oak Ridge, Tennessee, USA 10. https://doi.org/10.14291/tccon.ggg2014.documentation.R0/1221662.

Yang, Z., Toon, G.C., Margolis, J.S., Wennberg, P.O., 2002. Atmospheric /*coo* retrieved from ground-based near IR solar spectra. Geophys. Res. Lett. 29 (9), 53–1–53–4. https://doi.org/10.1029/2001GL014537. https://doi.org/10.1029/2001GL014537.

Zahnle, K., Arndt, N., Cockell, C., Halliday, A., Nisbet, E., Selsis, F., Sleep, N.H., 2007. Emergence of a habitable planet. Space Sci. Rev. 129, 35. https://doi.org/10.1007/s11214-007-9225-z.